

## **Calcium Transporter AtANN1 Mediates Cold-Induced Calcium Signaling and Plant Freezing Tolerance**

Qiangbo Liu<sup>1</sup>, Yanglin Ding<sup>1</sup>, Yiting Shi<sup>1</sup>, Liang Ma<sup>1</sup>, Yi Wang<sup>1</sup>, Chunpeng Song<sup>2</sup>, Katie A. Wilkins<sup>3</sup>, Julia M. Davies<sup>3</sup>, Heather Knight<sup>4</sup>, Marc R. Knight<sup>4</sup>, Zhizhong Gong<sup>1</sup>, Yan Guo<sup>1</sup>, Shuhua Yang<sup>1,\*</sup>

1 State Key Laboratory of Plant Physiology and Biochemistry, College of Biological Sciences, China Agricultural University, Beijing 100193, China

2 Institute of Plant Stress Biology, Collaborative Innovation Center of Crop Stress Biology, Henan University, Kaifeng 475001, China

3 Department of Plant Sciences, University of Cambridge, Cambridge CB2 3EA, UK

4 Department of Biosciences, Durham University, Durham DH1 3LE, UK

\*Correspondence author. Tel: +86-10-62734838; E-mail: yangshuhua@cau.edu.cn

**Running title:** AtANN1 mediates cold-induced Ca<sup>2+</sup> influx

**Keywords:** Calcium signal; calcium-permeable transporter AtANN1; OST1 kinase; freezing tolerance; *Arabidopsis*

## **Abstract**

The transient elevation of cytosolic free calcium concentration ( $[Ca^{2+}]_{\text{cyt}}$ ) induced by cold stress is a well-established phenomenon; however, the underlying mechanism remains elusive. Here, we report that the  $Ca^{2+}$ -permeable transporter ANNEXIN1 (AtANN1) mediates cold-triggered  $Ca^{2+}$  influx and freezing tolerance in *Arabidopsis thaliana*. The loss of function of *AtANN1* substantially impaired freezing tolerance, reducing the cold-induced  $[Ca^{2+}]_{\text{cyt}}$  increase and upregulation of the cold-responsive *CBF* and *COR* genes. Further analysis showed that the OST1/SnRK2.6 kinase interacted with and phosphorylated AtANN1, which consequently enhanced its  $Ca^{2+}$  transport activity, thereby potentiating  $Ca^{2+}$  signaling. Consistent with these results and freezing sensitivity of *ost1* mutants, the cold-induced  $[Ca^{2+}]_{\text{cyt}}$  elevation in the *ost1-3* mutant was observed to be reduced. Genetic analysis indicated that *AtANN1* acts downstream of *OST1* in responses to cold stress. Our data thus uncover a cascade linking OST1-AtANN1 to cold-induced  $Ca^{2+}$  signal generation, which activates the cold response and consequently enhances freezing tolerance in *Arabidopsis*.

## Introduction

Calcium ( $\text{Ca}^{2+}$ ), a universal second messenger, is involved in many aspects of plant development and responses to the environment. Abiotic and biotic stresses such as cold, heat, and salt, as well as pathogen infection, act on  $\text{Ca}^{2+}$ -permeable channels to cause transient increases in cytosolic free  $\text{Ca}^{2+}$  concentration ( $[\text{Ca}^{2+}]_{\text{cyt}}$ ). These  $\text{Ca}^{2+}$  signals (also known as  $\text{Ca}^{2+}$  signatures) convert external signals into diverse intracellular biochemical responses (Knight, 2002; Dodd *et al.*, 2010; Finka *et al.*, 2012; Tunc-Ozdemir *et al.*, 2013; Toyota *et al.*, 2018; Jiang *et al.*, 2019).

Low temperatures, with global climate change, are occurring more frequently and cause significant decreases in crop yield. Cold stress changes the fluidity of the plasma membrane, which may be sensed by  $\text{Ca}^{2+}$  channels and other plasma membrane proteins, triggering increased  $[\text{Ca}^{2+}]_{\text{cyt}}$  and activating cold stress responses (Zhu, 2016). A breakthrough study established that the G-protein regulator COLD1 (Chilling Tolerance Divergence 1), coupled with RGA1 (Rice G-protein  $\alpha$  Subunit 1), mediates the cold-induced influx of  $\text{Ca}^{2+}$  and confers cold sensing in rice (*Oryza sativa*) (Ma *et al.*, 2015; Guo *et al.*, 2018). However, it is unknown whether COLD1 itself functions as a  $\text{Ca}^{2+}$  channel or instead regulates the activity of a  $\text{Ca}^{2+}$  channel. In *Arabidopsis thaliana* seedlings, mechanosensitive  $\text{Ca}^{2+}$ -permeable channels MCA1 (*Mid1*-Complementing Activity 1) and MCA2 contribute to cold-induced influx of  $\text{Ca}^{2+}$  but are not the sole means of  $\text{Ca}^{2+}$  transport across the plasma membrane (Mori *et al.*, 2018). Therefore, although it is well established that cold stress triggers a transient elevation of  $[\text{Ca}^{2+}]$  in the cytosol and organelles of plant cells, it is not yet fully understood how the cold-induced  $\text{Ca}^{2+}$  signal is generated and controlled.

Annexins are a subfamily of phospholipid- and  $\text{Ca}^{2+}$ -binding proteins that are evolutionarily conserved across several kingdoms (Morgan *et al.*, 2006; Laohavisit & Davies, 2011). The *Arabidopsis* genome harbors eight genes encoding annexins (Cantero *et al.*, 2006), some of which regulate stress responses. Several studies have suggested that AtANN1 is a  $\text{Ca}^{2+}$ -permeable transporter that mediates the accumulation of  $[\text{Ca}^{2+}]_{\text{cyt}}$  in response to reactive oxygen species (ROS) and salt stresses (Lee *et al.*, 2004; Laohavisit *et al.*, 2012; Richards *et al.*, 2014). Cold induces

annexin expression in poplar leaves (Renaut *et al*, 2006). In wheat, two annexins accumulate at the plasma membrane in response to cold stress, and their insertion into the plasma membrane might be involved in regulating cold-induced  $\text{Ca}^{2+}$  signaling (Breton *et al*, 2000). AtANN1 is upregulated by heat treatment, and positively regulate the heat-induced increase in  $[\text{Ca}^{2+}]_{\text{cyt}}$  and heat tolerance (Wang *et al*, 2015). Annexins regulate the transcription factor MYB30-dependent  $\text{Ca}^{2+}$  signaling in response to oxidative and heat stresses (Liao *et al*, 2017). Moreover, AtANN1 interacts with AtANN4 in a  $\text{Ca}^{2+}$ -dependent manner to coordinately regulate drought and salt stress responses (Huh *et al*, 2010). A recent finding showed that AtANN4 regulates the generation of specific cytosolic  $\text{Ca}^{2+}$  signals under salt stress that are essential for activating the SOS (Salt Overly Sensitive) pathway (Ma *et al*, 2019). Moreover, the rice homolog, OsANN1, enhances heat tolerance by modulating the production of ROS (Qiao *et al*, 2015). Therefore, annexins function as  $\text{Ca}^{2+}$ -permeable transporters in regulating plant responses to adverse environmental cues.

When plants sense cold signal, they initiate comprehensive strategies that counteract the adverse effects of cold stress. One strategy is to biosynthesize protective substances, under the control of three key transcription factors in the CBF/DREB1 family (C-repeat Binding Factor/Dehydration-Responsive Element-Binding Factor1) (Thomashow, 1999; Jia *et al*, 2016; Zhao *et al*, 2016). CBF proteins bind directly to the promoters of *COR* (*Cold Regulated*) genes, some of which encode cryoprotective proteins or involve the accumulation of osmolytes that enhance plant freezing tolerance, and activate their expression (Stockinger *et al*, 1997; Liu *et al*, 1998; Thomashow, 1999). The expression of *CBFs* is rapidly induced by low temperatures, and the level of their expression is fine-tuned by many positive and negative regulators, including transcription factors, E3 ligases, SUMO E3 ligases, and protein kinases (Guo *et al.*, 2018; Liu *et al*, 2018a; Ding *et al*, 2020).

One of these protein kinases, OST1 (OPEN STOMATAL 1), known for its involvement in the plant's response to abscisic acid (ABA), was reported to positively regulate freezing tolerance in *Arabidopsis* (Mustilli *et al*, 2002; Ding *et al*, 2015).

ABA or cold can activate OST1 kinase activity by releasing the inhibition of type-2C protein phosphatases on OST1 in an ABA-dependent or independent manner, respectively (Ma *et al.*, 2009; Park *et al.*, 2009; Ding *et al.*, 2015; Ding *et al.*, 2019). Activated OST1 directly phosphorylates transcription factors localized at the nucleus such as ABRE-binding proteins/factors (AREBs/ABFs) or ICE1 (Inducer of *CBF* Expression 1), enhancing their transcriptional activity and thereby activating the expression of ABA- or cold-responsive genes, respectively (Furiihata *et al.*, 2006; Ding *et al.*, 2015). In addition, cold-activated OST1 interacts with and phosphorylates BTF3 (Basic Transcription Factor 3), BTF3L (BTF3-Like), and two U-box type E3 ligases (PUB25 and PUB26) in the nucleus, where it enhances BTF3(L)'s binding to and stabilization of CBF proteins and promotes the E3 activity of PUB25 and PUB26 (Ding *et al.*, 2018; Wang *et al.*, 2019). Furthermore, OST1 regulates stomatal movement by phosphorylating and activating the S-type anion channel SLAC1 and K<sup>+</sup> channel AKT1 at the plasma membrane (Lee *et al.*, 2009; Sato *et al.*, 2009). Together, these results indicate that OST1 plays key roles in regulating plant stress responses by participating in protein–protein interactions, enhancing the transcriptional or E3 activity of stress-responsive proteins, or activating channels at the plasma membrane.

In this study, we report that AtANN1 mediates the generation of cold-induced Ca<sup>2+</sup> signals. Mutation of *AtANN1* reduces the magnitude of the cold-induced increase in [Ca<sup>2+</sup>]<sub>cyt</sub> and consequently decreases freezing tolerance. Furthermore, AtANN1 positively regulates the expression of *CBFs* and their regulons. In addition, cold-activated OST1 phosphorylates AtANN1, thereby enhancing its Ca<sup>2+</sup> transport activity, and further potentiating Ca<sup>2+</sup> signaling. Our results thus unravel a critical link between OST1-AtANN1 and specific cold-triggered cytosolic Ca<sup>2+</sup> signals in plant responses to cold.

## Results

### AtANN1 positively regulate plant freezing tolerance

Previous studies showed that cold shock triggers transient increases in  $[Ca^{2+}]_{cyt}$ , which is mediated by  $Ca^{2+}$ -permeable channels. Annexins are suggested to be  $Ca^{2+}$ -permeable transporters (Laohavisit *et al.*, 2012; Ma *et al.*, 2019), and cold induces annexin gene expression in poplar (Renaut *et al.*, 2006) and protein accumulation of annexins at the plasma membrane in wheat (Breton *et al.*, 2000). Therefore, we hypothesized that annexins might be involved in regulating plant response to cold. To test this hypothesis, we first examined the freezing tolerance of *atann1* and *atann4* mutants, and found that *atann1* and *atann4* mutants exhibited decreased freezing tolerance compared to the wild type (Figs 1A, and EV1), indicating that annexins are indeed involved in regulating cold response in *Arabidopsis*.


The non-acclimated (NA) *atann1* loss-of-function mutant (SALK\_015426) (Lee *et al.*, 2004) displayed lower survival rate than the wild type (Figs 1A and B, EV1A and B). After cold acclimation (CA) at 4°C for 3 days, the *atann1* mutant also showed decreased freezing tolerance compared to the wild type (Fig 1A and B). Consistent with these results, the ion leakage, an indicator of membrane damage caused by freezing stress, was significantly increased in the *atann1* mutant under NA and CA conditions (Fig 1C). Furthermore, the freezing sensitive phenotype of the *atann1* mutant was fully rescued in two independent complementation lines harboring approximately 1.5 kb promoter and genomic DNA of *AtANN1* tagged with green fluorescence protein (GFP) (*atann1 AtANN1* #10 and *atann1 AtANN1* #4) (Figs 1A–C, and EV1A–E), indicating that this freezing sensitivity is indeed caused by mutation of *AtANN1*. These data suggest that *AtANN1* positively modulates constitutive (basal) and acquired freezing tolerance of *Arabidopsis*.

The *atann4-1* and *atann4-2* loss-of-function mutants (Ma *et al.*, 2019) exhibited lower survival rates than the wild type with or without cold acclimation (Fig EV1F and G). We then generated an *atann1 atann4-1* double mutant by crossing and examined its freezing tolerance. The non-acclimated *atann1 atann4-1* double mutant

phenocopied *atann1* and *atann4-1* single mutants, whereas the survival rate of the acclimated double mutant plants was lower than that of the single mutants (Fig EV1H and I), suggesting that AtANN1 and AtANN4 have redundant functions in acquired freezing tolerance. These results demonstrate that *AtANN1* and *AtANN4* are positive regulators of basal and acquired freezing tolerance in *Arabidopsis*.

To explore how AtANN1 regulates plant freezing tolerance, we examined the expression of *CBF* genes and CBF-regulated genes, including *GOLS3*, *COR15B*, *COR47*, and *KINI1*, in wild-type and *atann1* mutant plants under cold stress. The expression of these genes in wild-type and *atann1* mutant plants were comparable at 22°C (Fig 1D and E). However, cold-induction of *CBF1*, *CBF2* and *CBF3* was approximately 20-30% reduced in *atann1* mutant compared to the wild type (Fig 1D). Moreover, cold-induced expression of CBF target genes, *COR47* and *KINI1*, was decreased 35%, and *GOLS3* and *COR15B* was decreased up to 50% compared to the wild type (Fig 1E). These observations suggest that AtANN1 positively regulates plant acquired freezing tolerance at least partially by affecting the expression of *CBFs* and their target *COR* genes, with a more prominent effect on *COR* genes.

### **AtANN1 contributes to cold-induced elevation of $[Ca^{2+}]_{cyt}$**

AtANN1 was shown previously to act as a  $Ca^{2+}$ -permeable transporter (Laohavisit *et al.*, 2012), and cold shock induces a rapid increase in  $[Ca^{2+}]_{cyt}$  in *Arabidopsis* (Knight *et al.*, 1996). These findings prompted us to examine whether AtANN1 is involved in the cold shock-induced increase in  $[Ca^{2+}]_{cyt}$ . To this end, ten-day-old wild type and *atann1* mutant plants expressing aequorin, the  $Ca^{2+}$  reporter (Knight *et al.*, 1991), were treated with a  ice-cold water and subjected to luminescence measurements with a cold charge-coupled device (CDD) image system. After cold treatment, both wild type and *atann1* showed an increase in luminescence signals. However, the luminescence signal intensity in *atann1* was less half of that in wild type (Fig EV2A and B), although the aequorin protein levels in *atann1* and wild type were comparable (Fig EV2C).

Next, the  $[Ca^{2+}]_{cyt}$  changes in wild type and *atann1* after cold shock was

measured with a luminometer.  $[Ca^{2+}]_{cyt}$  was rapidly and dramatically induced by cold water (Fig 2A and B). However, the *atann1* mutant showed a lower cold shock-induced increase in  $[Ca^{2+}]_{cyt}$  than the wild type (Fig 2A and B). The cold shock-induced  $[Ca^{2+}]_{cyt}$  elevation in the *ann1-2* mutant (SAIL\_414\_C01) expressing aequorin (Wang *et al.*, 2015) was also diminished compared to that of the wild type (Fig EV2D). Moreover, the change of  $[Ca^{2+}]_{cyt}$  in the *atann1* mutant was fully complemented by a genomic fragment of AtANN1 tagged with GFP (*atann1 AtANN1* #10) (Figs 2A and B, EV2A and B). After treating the plants with lanthanum chloride ( $LaCl_3$ ), a widely used  $Ca^{2+}$  channel blocker, we found that the cold shock-induced  $[Ca^{2+}]_{cyt}$  increase in wild type, *atann1* and *atann1 AtANN1* complementation plants was dramatically suppressed (Fig 2A and B). However, treatment with water at room temperature (22°C) did not obviously alter the  $[Ca^{2+}]_{cyt}$  in the presence or absence of  $LaCl_3$  (Fig EV2E).

We also measured  $[Ca^{2+}]_{cyt}$  in *atann4-1* mutant expressing aequorin with and without cold shock, and observed a similar scenario as noted for *atann1*: the cold shock-induced increase in  $[Ca^{2+}]_{cyt}$  was lower in *atann4-1* than in the wild type (Fig EV2F). Together, these results indicate that AtANN1 and AtANN4 are important for mediating a rapid increase in  $[Ca^{2+}]_{cyt}$  upon cold stress.

### **AtANN1 interacts with OST1**

We further dissected the effects of cold stress on *AtANN1* mRNA and AtANN1 protein levels, and found that *AtANN1* transcript levels and protein levels were not obviously affected by cold stress (Appendix Fig S1A and B).

To explore how AtANN1 functions in cold response, we pursued to identify the interacting proteins of AtANN1. In our previous liquid chromatography-tandem mass spectrometry (LC-MS/MS) analysis using transgenic plants overexpressing *OST1-Myc* to identify OST1-interacting proteins (Ding *et al.*, 2015; Ding *et al.*, 2018), AtANN1 was one of the candidate interacting proteins (Appendix Table S1). To verify the interaction between AtANN1 and OST1, we performed yeast two-hybrid assays, and observed that AtANN1 interacted with OST1 in yeast cells (Fig EV3A and



B). AtANN1 has four annexin repeat domains (A1-A4). When A1, A12, A34, or A4 were deleted, the truncated proteins could interact with OST1 in yeast; however, the truncated protein failed to interact with OST1 when the first three domains were deleted (Fig EV3A and B). These results suggest that any one of the first three annexin repeat domains are sufficient for their interaction in yeast. *In vitro* pull-down assays showed that GST-OST1, but not GST, pulled down MBP-His-AtANN1 protein (Fig 2C). Interestingly, we found that OST1<sup>G33R</sup>, a form of OST1 with no kinase activity (Belin *et al*, 2006), failed to directly interact with MBP-His-AtANN1 *in vitro* (Fig 2C), possibly due to the lost kinase activity or conformation change caused by this mutation of OST1.

A recent study revealed that AtANN1-GFP was enriched at the plasma membrane and vesicles of non-dividing cells and in the mitotic and cytokinetic microtubular arrays of dividing cells. Furthermore, AtANN1-GFP was localized to the cytoplasmic strands of pavement and stomatal guard cells of the leaf epidermis (Ticha *et al*, 2020) (Appendix Fig S1C), overlapping with the reported localization of OST1 (Belin *et al.*, 2006). These data suggest that that AtANN1 and OST1 might interact *in vivo*. We then performed co-immunoprecipitation (co-IP) assays using proteins extracted from *Nicotiana benthamiana* leaves co-expressing *AtANN1-GFP/OST1-Myc*, *AtANN1-GFP/OST1<sup>G33R</sup>-Myc*, and *AtANN1-GFP/Myc*, and further confirmed that AtANN1-GFP interacts with OST1-Myc, but not with OST1<sup>G33R</sup>-Myc in plants (Fig 2E). *In planta* interaction between AtANN1 and OST1 was confirmed by bimolecular fluorescence complementation (BiFC) assays in *N. benthamiana* epidermal cells confirmed the AtANN1-OST1 interaction signals were overlapped with PIP2-mcherry signals, a marker of plasma membrane (Entzian & Schubert, 2016) (Fig 2D). However, no interaction was observed between AtANN1 and OST1<sup>G33R</sup> (Fig 2D), although the respective fusion proteins were properly expressed (Fig EV3C). Furthermore, AtANN4 was shown to interact with OST1 *in vitro* and *in vivo* (Fig EV3D and E).

To examine whether the interaction between AtANN1 and OST1 is influenced by cold stress, we performed co-IP assay using *OST1-Myc* transgenic plants before and after cold treatment. Anti-Myc agarose beads were used for IPed OST1-Myc, and

anti-AtANN1 antibody was used to detect AtANN1 protein. Wild-type Col-0 was used as a control. We observed that AtANN1 was associated with OST1, and that this association was enhanced by treatment at 4°C (Fig 2E and F). This result was further verified by co-IP assays using *Nicotiana benthamiana* leaves expressing both *OST1-Myc* and *AtANN1-GFP* with and without cold treatment (Fig 2G). Taken together, these data indicate that AtANN1 interacts with OST1 in plants, and that this interaction is promoted under cold stress.

### ***AtANN1* acts downstream of *OST1* to positively regulate freezing tolerance**

To determine the genetic interaction between *OST1* and *AtANN1*, we generated *ost1-3 atann1* mutants by crossing *ost1-3* and *atann1* single mutants, and performed freezing tolerance assays. The *ost1-3* and *atann1* single mutants displayed freezing hypersensitivity compared to the wild type under both acclimation and non-acclimation conditions (Fig 3A–C). The *ost1-3 atann1* double mutants showed no greater decrease in freezing tolerance than that observed in *atann1* and *ost1-3*, indicating the effects of the two mutations were not additive (Fig 3A–C). Furthermore, we generated *OST1-Myc atann1* by crossing *OST1-Myc* transgenic plants with *atann1* mutant (Fig 3D and E). We found that *OST1-Myc* transgenic plants exhibited enhanced freezing tolerance, which is consistent with the previous study (Ding *et al.*, 2015). However, overexpression of *OST1* failed to rescue the freezing sensitivity of *atann1* (Fig 3F–H). These results collectively reveal that *AtANN1* acts downstream of *OST1* to positively regulate the plant freezing tolerance.

### **OST1 phosphorylates AtANN1 under cold stress**

Given that OST1 interacts with AtANN1 and AtANN4, we asked whether OST1 phosphorylates AtANN1 and AtANN4. *In vitro* phosphorylation assays showed that AtANN1 and AtANN4 were directly phosphorylated by OST1 (Fig 4A and B). We also performed in-gel kinase assays using GST-AtANN1 as the substrate and total proteins extracted from wild-type Col-0 and the *ost1-3* knockout mutant with or without cold treatment. OST1 kinase activity was clearly detected in wild type Col-0

but not in *ost1-3* mutant after cold treatment when GST-AtANN1 served as the substrate (Fig 4C), suggesting that the cold-activated OST1 phosphorylates AtANN1.

To further determine the phosphorylation residues of AtANN1 by OST1, we first generated a series of mutant constructs that inactivated each conserved putative phosphorylation site in AtANN1 with a serine/threonine to alanine substitution (AtANN1<sup>S101A</sup>, AtANN1<sup>S194A</sup>, AtANN1<sup>S289A</sup>, AtANN1<sup>T116A</sup>, and AtANN1<sup>T270A</sup>), and performed *in vitro* phosphorylation assays using these mutated proteins as substrates. Compared to the wild type AtANN1, the phosphorylation of AtANN1<sup>S101A</sup>, AtANN1<sup>S194A</sup>, AtANN1<sup>T116A</sup>, and AtANN1<sup>T270A</sup> by OST1 was decreased to different extent, whereas the phosphorylation of AtANN1<sup>S289A</sup> was largely abolished (Fig 4D). These assays suggested that S289 is a major residue for phosphorylation of AtANN1 by OST1, and the other four residues may have a minor contribution to the AtANN1 phosphorylation by OST1. *In vitro* LC-MS/MS assays further confirmed the phosphorylation of AtANN1<sup>S289</sup> by OST1 (Appendix Fig S2A).

We then performed a LC-MS/MS assay using *AtANN1-Myc* and *AtANN1-Myc ost1-3* transgenic plants before and after cold treatment to determine whether AtANN1 is phosphorylated by OST1 *in vivo*. AtANN1 was phosphorylated at Ser289 in the *AtANN1-Myc* transgenic plants after cold treatment at 4°C for 10, 30 and 120 min, but not in the *AtANN1-Myc* transgenic plants without cold treatment or in the *AtANN1-Myc ost1-3* transgenic plants with or without cold treatment (Figs 4E, and Appendix S2B). Taken together, these data collectively suggest that OST1 phosphorylates AtANN1 predominantly at Ser289 under cold conditions.

To dissect the biological function of AtANN1 phosphorylation in plants, we transformed the *atann1* mutant with *AtANN1:AtANN1<sup>S289A</sup>-GFP* and *AtANN1:AtANN1<sup>S289E</sup>-GFP* (carrying the serine to glutamine mutation, a phosphomimic form of AtANN1), and examined the freezing tolerance of these transgenic plants. Both gene expression and protein analyses showed that they were expressed (Appendix Fig S2C and D). Like the wild-type *AtANN1* (Fig 1A–C), the survival rate and ion leakage of *atann1* were fully rescued by the phosphomimic form *AtANN1<sup>S289E</sup>* in two independent *atann1 AtANN1<sup>S289E</sup>* lines (#5 and #7) (Figs 5A–C,

and Appendix Fig S3), but were not complemented by the non-phosphorylatable form *AtANN1*<sup>S289A</sup> after freezing treatment (Figs 5D–F, and Appendix Fig S4). These data suggest that phosphorylation of AtANN1 at Ser289 is required for its function in regulating freezing tolerance.

### **The Ca<sup>2+</sup> transport activity of AtANN1 is enhanced by OST1**

Next, we next examined whether OST1 can modulate the Ca<sup>2+</sup> transport activity of AtANN1, using electrophysiological assays of AtANN1 in *Xenopus* oocytes microinjected with *AtANN1* cRNA. Because Ba<sup>2+</sup> has been used extensively for Ca<sup>2+</sup> channel identification (Hamilton *et al*, 2000; Pei *et al*, 2000; Zhang *et al*, 2007), we used Ba<sup>2+</sup> as the major charge-carrying ion to measure Ca<sup>2+</sup> channel-like activity in the electrophysiological assays.

Control oocytes injected with ddH<sub>2</sub>O alone did not produce obvious currents, with or without 30 mM Ba<sup>2+</sup> in the bathing solution, and oocytes injected with *AtANN1* alone likewise failed to elicit currents in the absence of Ba<sup>2+</sup> (Fig 6A and B). In the presence of 30 mM Ba<sup>2+</sup>, however, expression of *AtANN1* produced substantial currents (Fig 6A and B). In addition, the currents produced by AtANN1 were fully blocked by LaCl<sub>3</sub> (Fig 6A and B). These data suggest that AtANN1 has Ca<sup>2+</sup> transport activity in *Xenopus* oocytes, which is consistent with the previous findings for AtANN1 in root cells (Laohavisit *et al.*, 2012). The Ba<sup>2+</sup> currents produced in *Xenopus* oocytes co-expressing AtANN1 and OST1 were greater than those produced by expression of AtANN1 alone (Fig 6A–C), and similar results were obtained when 30 mM Ca<sup>2+</sup> was used instead of Ba<sup>2+</sup> (Fig EV4A-C). These data indicate that OST1 enhances the Ca<sup>2+</sup> transport activity of AtANN1.

We next examined whether phosphorylation of AtANN1 by OST1 is the mechanism by which OST1 enhances AtANN1's Ca<sup>2+</sup> transport activity. To test this possibility, we performed electrophysiological assays on *Xenopus* oocytes expressing AtANN1, AtANN1<sup>S289A</sup>, OST1/AtANN1, and OST1/AtANN1<sup>S289A</sup>. Both AtANN1 and AtANN1<sup>S289A</sup> had Ca<sup>2+</sup> transport activity; however, the transport activity of AtANN1, but not AtANN1<sup>S289A</sup>, was enhanced by OST1 (Fig 6D–F). These data

demonstrate that OST1 phosphorylates AtANN1 to enhance its Ca<sup>2+</sup> transport activity.

We next examined whether OST1 regulates Ca<sup>2+</sup> influx in response to cold stress by measuring Ca<sup>2+</sup> levels in wild-type and *ost1-3* mutant plants expressing aequorin with or without cold shock. There was no obvious difference of the [Ca<sup>2+</sup>]<sub>cyt</sub> in wild-type and *ost1-3* mutant without cold shock (Fig EV4D). However, the [Ca<sup>2+</sup>]<sub>cyt</sub> was significantly lower in the *ost1-3* mutant than in the wild type after cold treatment (Fig 7A and B). Moreover, the cold shock-induced increase in [Ca<sup>2+</sup>]<sub>cyt</sub> was also inhibited by LaCl<sub>3</sub> (Fig 7A and B). These results collectively support the idea that OST1 regulates the cold-induced increase in [Ca<sup>2+</sup>]<sub>cyt</sub> at least partially by phosphorylating the Ca<sup>2+</sup>-permeable transporter AtANN1.

Previous studies suggest that the Ca<sup>2+</sup>-binding affinity of annexins is regulated by their phosphorylation state (Konopka-Postupolska *et al*, 2011; Ma *et al.*, 2019). We thus examined whether the mutation of S289 of AtANN1 affects its Ca<sup>2+</sup>-binding activity using Microscale Thermophoresis (MST) assays. The non-phosphorylatable form GST-AtANN1<sup>S289A</sup> had reduced Ca<sup>2+</sup>-binding activity, whereas the phosphomimic form GST-AtANN1<sup>S289E</sup> had slightly enhanced Ca<sup>2+</sup>-binding activity compared to GST-AtANN1 (Figs 7C, and EV4E). Therefore, it appears that phosphorylation of AtANN1 at S289 modulates its Ca<sup>2+</sup>-binding affinity; however, we cannot exclude the possibility that the reduced binding affinity of Ca<sup>2+</sup>-AtANN1<sup>S289</sup> might be caused by conformational changes of AtANN1 resulting from this mutation.

## Discussion

Cold stress causes a dramatic and rapid increase in  $[Ca^{2+}]_{cyt}$ , which is required for proper *COR* gene expression (Knight *et al.*, 1991; Knight *et al.*, 1996). In this study, we report that the  $Ca^{2+}$  transporter AtANN1 is involved in cold-induced elevation of  $[Ca^{2+}]_{cyt}$ . Biochemical and genetic evidence demonstrates that plasma membrane-localized AtANN1 mediates rapid  $Ca^{2+}$  influx from apoplastic  $Ca^{2+}$  stores into the cytosol under cold stress, and positively regulates *COR* expression and plant tolerance to freezing stress. In addition, OST1 is activated under cold stress and phosphorylates AtANN1 at Ser289, which enhances its  $Ca^{2+}$  transport activity, thereby potentially amplifying the  $Ca^{2+}$  signaling (Fig 7D).

It is well established that the transient  $[Ca^{2+}]_{cyt}$  elevation in plants occurs seconds after cold shock (Knight *et al.*, 1991); however, due to the relatively low sensitivity of in-gel kinase assays, the cold-activated OST1 activity was barely detected within 30 min using this assay. Therefore, we instead used an IP-MS/MS assay to assess OST1-mediated AtANN1 phosphorylation *in planta*. We detected phosphorylation at Ser289 of AtANN1 in the 10-min cold-treated *AtANN1-Myc* plants, but not in the non-treated plants or in the *AtANN1-Myc ost1-3* plants with or without cold treatment. These results suggest that OST1-mediated phosphorylation of AtANN1 occurs within several minutes or possibly even within less time. OST1 has basal kinase activity under normal conditions (Ding *et al.*, 2015), and this basal activity may also function in regulating AtANN1 activity. In addition, a previous study showed that continuous cold stimulation induces a biphasic increase in  $[Ca^{2+}]_{cyt}$ , with the first peak occurring within several seconds and second at several minutes (Short *et al.*, 2012). Therefore, we propose that, besides affecting the first transient increase in  $[Ca^{2+}]_{cyt}$ , cold-activated OST1 phosphorylates and enhances the  $Ca^{2+}$  transport activity of AtANN1, which consequently magnifies the second  $[Ca^{2+}]_{cyt}$  elevation under cold stress. Alternatively, considering that the cold-induced cytoplasmic  $Ca^{2+}$  influx exhibits diurnal variation in guard cells, and circadian modulation of cold-induced whole plant  $[Ca^{2+}]_{cyt}$  increases is correlated to the circadian pattern of *RD29A* induction (Dodd *et al.*, 2006), it is possible cold-activated OST1 regulates

AtANN1-mediated cytosolic calcium oscillations or circadian oscillations in the guard cells or whole plant under long-term cold treatment. These hypotheses await further investigation. Our in-gel kinase assay suggested that AtANN1 can also be phosphorylated by kinases other than OST1, possibly including other SnRK2s and CRPK1 (around 43kDa) (Liu *et al.*, 2017) and RAF2 (around 100kDa). Three recent studies reported that RAF-mediated activation of OST1 is required for ABA signaling and the osmotic stress response (Lin *et al.*, 2020; Soma *et al.*, 2020; Takahashi *et al.*, 2020). Future studies should examine whether these kinases mediate AtANN1 phosphorylation and thereby modulate its Ca<sup>2+</sup> transport activity under cold conditions.

Annexins have phospholipid- and Ca<sup>2+</sup>-binding activities that are important for plant responses to stress (Morgan *et al.*, 2006; Laohavisit & Davies, 2011). Previous studies demonstrated that AtANN1 acts as a Ca<sup>2+</sup>-permeable channel-like transporter with a role in regulating Ca<sup>2+</sup> influx into the cytosol under salt- and oxidative-stress conditions (Lee *et al.*, 2004; Laohavisit *et al.*, 2012; Richards *et al.*, 2014). AtANN4 was shown to promote Ca<sup>2+</sup> influx under salt stress to activate the SOS pathway (Ma *et al.*, 2019). In this study, we established that AtANN1 also functions as a Ca<sup>2+</sup>-permeable channel-like transporter in the plant response to cold stress. It should be noted that the cold-induced increase in [Ca<sup>2+</sup>]<sub>cyt</sub> is not fully repressed in the *atann1* mutant. This may be due to functional redundancy, as AtANN1 has seven homologs in *Arabidopsis* (Cantero *et al.*, 2006). Indeed, we established that AtANN4 also modulates the cold-induced increase in [Ca<sup>2+</sup>]<sub>cyt</sub> and freezing tolerance. It is worth noting that the *Arabidopsis* genome includes over 40 genes encoding putative Ca<sup>2+</sup> channels (Ward *et al.*, 2009). A previous study demonstrated that the Ca<sup>2+</sup>-permeable mechanosensitive channels MCA1 and MCA2 mediate Ca<sup>2+</sup> influx under cold stress (Mori *et al.*, 2018). Therefore, some other Ca<sup>2+</sup>-permeable transporters or channels may also regulate Ca<sup>2+</sup> influx under cold stress.

Besides having Ca<sup>2+</sup>-binding activity, plant annexins have sequences that strongly resemble the heme-binding region of horseradish peroxidase, suggesting that they might also have peroxidase activity (Gorecka *et al.*, 2005; Laohavisit *et al.*, 2009;

Qiao *et al.*, 2015). In addition, overexpression of *OsANN1* enhances thermotolerance by regulating H<sub>2</sub>O<sub>2</sub> content and redox homeostasis (Qiao *et al.*, 2015). These results suggest that the peroxidase activity of annexins may be important for their functions in plant responses to abiotic stress. In this study, we established that AtANN1 not only mediates cold acclimation in a CBF-dependent manner, but also mediates basal freezing tolerance in *Arabidopsis*. However, the mechanism by which AtANN1 regulates basal freezing tolerance is unknown. Considering that plant annexins might have peroxidase activity and the ROS play key roles in plant basal freezing tolerance (Laohavisit *et al.*, 2009; Costa-Broseta *et al.*, 2018), it is possible that AtANN1 positively regulates plant basal freezing tolerance by inhibiting ROS overproduction.

Expression of the cold-regulated gene *KINI* is regulated by Ca<sup>2+</sup> influx under cold stress (Knight *et al.*, 1996). Here we showed that loss of *AtANN1* decreases the cold-induced expression of *CBFs* and their downstream genes, *GOLS3*, *COR15B*, *COR47* and *KINI*. These results further support the importance of Ca<sup>2+</sup> for cold-responsive gene expression. However, it remains unclear how the AtANN1-mediated Ca<sup>2+</sup> signal regulates cold-responsive gene expression. The *Arabidopsis* genome encodes many calmodulin (CaM)-binding proteins (Reddy *et al.*, 2011; Viridi *et al.*, 2015; Edel *et al.*, 2017), any of which could be involved in transducing the Ca<sup>2+</sup> signal. CaM has two Ca<sup>2+</sup>-binding domains, each consisting of paired EF-hands, one at the N-terminus and the other at the C-terminus (Finn & Forsen, 1995). Some transcription factors (TFs) bind to Ca<sup>2+</sup>-CaM, which allows the TFs to sense Ca<sup>2+</sup> signals through a Ca<sup>2+</sup>-CaM-TF module. This mechanism may rapidly translate Ca<sup>2+</sup> signals induced by environmental cues into changes in gene expression. In *Arabidopsis*, CAMTA (Calmodulin-binding transcription activator) family members, particularly CAMTA3, have been reported to regulate plant freezing tolerance by activating *CBF* expression (Doherty *et al.*, 2009; Kim *et al.*, 2013; Kidokoro *et al.*, 2017). It will be interesting to explore whether Ca<sup>2+</sup> regulates CAMTA activity and whether CAMTA3 plays a role in modulating cold-responsive gene expression mediated by AtANN1. In addition to TFs, several Ca<sup>2+</sup>-binding proteins, such as CDPKs (Ca<sup>2+</sup>-dependent protein kinases), CBLs (Calcineurin B-like



proteins), and CIPKs (CBL-interacting protein kinases), are reported to be involved in cold tolerance in plants (Kim *et al.*, 2003; Liu *et al.*, 2008; Liu *et al.*, 2018b; Zhang *et al.*, 2019). Whether these proteins are responsible for decoding specific cold-induced  $\text{Ca}^{2+}$  signals merits further investigation.

Calcium spiking is a distinct behavior characterized by sharp increases in  $[\text{Ca}^{2+}]_{\text{cyt}}$  induced by abiotic and biotic stress, followed by decreases back to the basal level, even in the continued presence of the stimulus (Kudla *et al.*, 2018). Therefore, the activity of calcium channels or transporters should be tightly controlled in plants. We found that the AtANN1 activity is promoted by OST1 under cold stress; however, it remains unknown how its activity is blocked in the attenuate stage. Upon long exposure of salt stress, SOS2-mediated phosphorylation of AtANN4 was shown to be promoted by SCaBP8, which enhances the AtANN4-SCaBP8 interaction, thereby consequently repressing AtANN4 activity (Ma *et al.*, 2019). Recent findings have provided evidence that the activities of  $\text{Ca}^{2+}$  channels are controlled by CaMs and protein kinases (Ma *et al.*, 2019; Tian *et al.*, 2019; Yu *et al.*, 2019). Moreover, the expression of *AtANN* genes are negatively regulated by MYB30 in response to heat stress (Liao *et al.*, 2017). These findings may provide us with a strategy to study the mechanism by which  $\text{Ca}^{2+}$  transport activity of AtANN1 is repressed under non-stress conditions.

## Materials and Methods

### Plants materials and growth conditions

The *Arabidopsis thaliana* ecotype Columbia and all plants used in this study were grown on Murashige and Skoog (MS) medium (Sigma-Aldrich) containing 0.8% (w/v) agar and 2% (w/v) sucrose at 22°C under long-day conditions (16-h light/8-h dark cycle). T-DNA insertion mutants, *atann1* (Salk\_015426) (Lee *et al.*, 2004; Laohavisit *et al.*, 2012), *ann1-2* mutant (SAIL\_414\_C01) (Wang *et al.*, 2015), *atann4-1* and *atann4-2* (Ma *et al.*, 2019), and *ost1-3* (Salk\_008068) (Ding *et al.*, 2015), were used in this study. In addition, wild-type Col-0, *atann1* mutants and the *atann1* complemented line (*Atann1AtANN1* #10) harboring aequorin were described previously (Laohavisit *et al.*, 2012; Wang *et al.*, 2015). *ost1-3* mutant harboring aequorin was generated by crossing *ost1-3* with wild-type Col-0 plants harboring aequorin described (Knight *et al.*, 1991).

### Plasmid construction and plant transformation

*AtANN1* cDNA was amplified by PCR (polymerase chain reaction) and cloned into *pSuper1300*, *pGEX-6P-1*, *pMAL-c2*, *YFP<sup>C</sup>* (based on *pGEMHE* vector) and *pGADT7* vectors to generate *Super:AtANN1-Myc*, *Super:AtANN1-GFP*, *GST-AtANN1*, *MBP-His-AtANN1*, *AtANN1-YFP<sup>C</sup>* and *AtANN1-pGADT7* (*AtANN1-AD*) constructs, respectively. *AtANN1* promoter fragment (1,566 bp) together with its genomic DNA was amplified and fused with GFP in the *pCAMBIA1300* vector to obtain the desired constructs, *AtANN1:AtANN1-GFP*, *AtANN1:AtANN1<sup>S289A</sup>-GFP* (carrying a S289A mutation of *AtANN1*) and *AtANN1:AtANN1<sup>S289E</sup>-GFP* (carrying a S289E mutation of *AtANN1*).

Using *AtANN1-pGEX-6P-1* plasmid as a template, site-directed mutagenesis was carried out to obtain the mutated forms of *AtANN1*. They were amplified and cloned into *pGEX-6P-1* vector to generate *GST-AtANN1<sup>S101A</sup>*, *GST-AtANN1<sup>S194A</sup>*, *GST-AtANN1<sup>S289A</sup>*, *GST-AtANN1<sup>T116A</sup>* and *GST-AtANN1<sup>T270A</sup>* constructs.

*OST1* cDNA was amplified and cloned into *pMAL-c2* to obtain *MBP-His-OST1* constructs. Using *OST1-pGEX-4T-1*, *OST1-YNE* and *Super:OST1-Myc* (Ding *et al.*,

2015) constructs as templates, site-directed mutagenesis was performed to generate the kinase dead form of OST1. Then they were amplified and cloned into *pGEX-4T-1*, *pSPYNE-35S* or *pSuper1300* to create *OST1<sup>G33R</sup>-pGEX-4T-1*, *OST1<sup>G33R</sup>-YNE* and *Super:OST1<sup>G33R</sup>-Myc* constructs. All primers used were listed in Appendix Table S2, and all vectors and constructs were listed in Appendix Table S3.

The *Agrobacterium tumefaciens* strain GV3101, which was transformed into the related constructs, was transformed into *Arabidopsis* plants. *AtANN1:AtANN1-GFP*, *AtANN1:AtANN1<sup>S289A</sup>-GFP* and *AtANN1:AtANN1<sup>S289E</sup>-GFP* constructs were transformed into the *atann1* mutant. The transgenic plants were selected on MS medium containing hygromycin B. T3 or T4 homozygous transgenic plants were used in this study.

*atann1 AtANN1* plants were transformed by floral dip to express cytosolic (apo)aequorin driven by the 35S promoter. The pGreen vector based on pMAQ containing 35S:Aequorin was transferred into *Agrobacterium tumefaciens* GV3101 (Knight *et al.*, 1991). All plants used in aequorin assays were at least three generations post-transformation and discharge levels were equivalent across genotypes.

### **[Ca<sup>2+</sup>]<sub>cyt</sub> determination**

The [Ca<sup>2+</sup>]<sub>cyt</sub> determination assays were performed as previously described (Liao *et al.*, 2017) with some modifications. The 10-d-old seedlings grown on MS medium were used for [Ca<sup>2+</sup>]<sub>cyt</sub> determination. First, the seedlings were soaked in 200 µL coelenterazine solution (final concentration 10 µM, 1% [v/v] ethanol, and 0.1% [v/v] Triton X-100) in 1.5 mL tubes for 5 h at 22°C in the dark (Knight *et al.*, 1991). Experiments were performed without liquid in the tubes. Luminescence counts were recorded every 1 s. After 10 s of counting, 200 µL of ice-cold water was injected into the tube in the luminometer sample housing. After 120 s of counting, the remaining aequorin was discharged by the addition of 200 µL discharge solution (containing 2 M CaCl<sub>2</sub> and 20% [v/v] ethanol) for 120 s. The quantification of [Ca<sup>2+</sup>]<sub>cyt</sub> was performed as described (Rentel & Knight, 2004).

### **Freezing tolerance and ion leakage assays**

The freezing tolerance and ion leakage assays were performed as previously described (Ding *et al.*, 2015) with some modifications. Briefly, 12-d-old *Arabidopsis* seedlings grown on MS medium were treated with or without cold acclimation at 4°C for 3 d and then put into a freezing chamber (RUMED4501) when its temperature reached 0°C. Then the temperature dropped by 1°C per hour until the desired temperature was reached. After freezing treatment, the seedlings were transferred to 4°C chamber in the dark for 12 h and then transferred to normal conditions for 3 d for recovery. The survival rates of the seedlings were counted by the ratio of the number of living seedlings to the number of total seedlings.

After 3-d recovery, seedlings were soaked in 5 mL deionized water (sample S0) in 15 mL tubes, which were shaken at 22°C for 1 h. After that, the electrical conductivity was detected as S1. Next, the samples were heated at 100°C for 1 h, followed by shaking at 22°C for 1 h; the electrical conductivity was measured as S2. The ion leakage was calculated as  $(S1-S0)/(S2-S0) \times 100\%$ .

### **Quantitative real-time PCR (qPCR) analysis**

Total RNA was extracted with TRIzol reagent (Invitrogen) from 12-d-old *Arabidopsis* seedlings grown on MS medium with or without cold treatment. Total RNA (3 µg) was treated with RNase-free *DNase* I (Takara) to remove genomic DNA and then reverse-transcribed with the M-MLV reverse transcriptase (Promega). Quantitative real-time PCR was carried out using SYBR Green PCR Master Mix (Takara) on a 7500 Real-Time PCR system (Applied Biosystems). The method for calculating gene expression was performed as described (Shi *et al.*, 2012).

### **Yeast two-hybrid assays**

The yeast two-hybrid assays were performed as described (Ding *et al.*, 2015). In brief, *AtANN1-pGADT7* and *OST1-pGBKT7*, *AtANN1-ΔA1-pGADT7* and *OST1-pGBKT7*, *AtANN1-ΔA12-pGADT7* and *OST1-pGBKT7*, *AtANN1-ΔA123-pGADT7* and

*OST1-pGBKT7*, *AtANN1-ΔA34-pGADT7* and *OST1-pGBKT7*, *AtANN1-ΔA4-pGADT7* and *OST1-pGBKT7*, *AtANN1-pGADT7* and *pGBKT7* or *OST1-pGBKT7* and *pGADT7* were transformed into the yeast strain AH109. The yeast cells were grown on SC–Leu–Trp (Clontech, 2 d at 28°C) or SC–Leu–Trp–His medium supplemented with 2 mM 3-AT (Clontech, 4 d at 28°C).

### ***In vitro* pull-down assays**

The pull-down assays were performed as described (Ding *et al.*, 2015). Purified GST-OST1, GST-OST1<sup>G33R</sup> or GST proteins (10 μg) were incubated with GST agarose beads in PBS buffer containing 0.3% [v/v] NP-40 (pull-down binding buffer) at 4°C for 2 h and then washed with pull-down binding buffer. The immunoprecipitated GST-OST1, GST-OST1<sup>G33R</sup> or GST was incubated with 2 μg MBP-His-AtANN1 at 4°C for 2 h in pull-down binding buffer. After five washes, the proteins were analyzed by immunoblot analysis. Anti-His antibody (Beijing Protein Innovation, #AbM59012-18-PU) was used to detect MBP-His-AtANN1, and anti-GST antibody (Beijing Protein Innovation, #AbM59001-2H5-PU) was used to detect GST-OST1 and GST-OST1<sup>G33R</sup>.

### **Co-immunoprecipitation (Co-IP) assays**

The co-IP assays were performed as previously described (Ding *et al.*, 2015). In short, the total proteins were extracted from *N. benthamiana* leaves expressing *Super:AtANN1-GFP/Super:OST1-Myc*, *Super:AtANN1-GFP/Super:OST1<sup>G33R</sup>-Myc* or *Super:AtANN1-GFP/Super:Myc* constructs with protein extraction buffer (50 mM Tris-HCl pH 7.5, 150 mM NaCl, 10 mM MgCl<sub>2</sub> and 0.1% [v/v] Triton X-100) and then incubated with anti-Myc agarose (Sigma-Aldrich, #A7470) for 2 h at 4°C. After washing by protein extraction buffer for five times, the co-immunoprecipitated products were separated by SDS-PAGE and detected with anti-Myc (Sigma-Aldrich, #M4439) and anti-GFP (Abmart, #M20004H) antibodies.

### **Bimolecular fluorescence complementation (BiFC) assays**

The constructs *OST1-YNE* and *AtANN1-YCE* or *OST1<sup>G33R</sup>-YNE* and *AtANN1-YCE* were transfected into *N. benthamiana* leaves for transient expression. The YFP fluorescence signal was detected by using a confocal microscope after 3-d infiltration.

### ***In vitro* protein kinase assays**

*In vitro* kinase assays were performed as previously described (Ding *et al.*, 2015). The purified proteins MBP-His-OST1 together with GST-AtANN1 or GST were incubated with kinase reaction buffer containing 20 mM MgCl<sub>2</sub>, 50 mM Tris-HCl pH 7.5, 1 mM DTT, 50 μM ATP, and 1 μCi [ $\gamma$ -<sup>32</sup>P] ATP at 30°C for 30 min and then heated at 100°C for 5 min with 5× loading buffer. The proteins were analyzed by SDS-PAGE and detected by Typhoon 9410 imager. Coomassie brilliant blue was used as a loading control.

### **In-gel kinase assays**

In-gel kinase assays were performed as previously described (Ding *et al.*, 2015). Total proteins were extracted from 12-d-old seedlings (control or exposed to 4°C) in protein extraction buffer containing 5 mM EDTA pH 8.0, 5 mM EGTA pH 8.0, 25 mM NaF, 1 mM Na<sub>3</sub>VO<sub>4</sub>, 20% [v/v] glycerol, 2 mM DTT, 1× protease inhibitor cocktail (Roche) and 25 mM HEPES-KOH pH 7.5. Then, the proteins were separated on a 10% [v/v] SDS-PAGE gel containing 0.2 mg/mL GST-AtANN1. Then, the gel was washed three times with washing buffer (25 mM Tris-HCl pH 7.5, 0.5 mM DTT, 5 mM NaF, 0.1 mM Na<sub>3</sub>VO<sub>4</sub>, 0.5 mg/mL BSA and 0.1% [v/v] Triton X-100) at 22°C for 20 min each. The gel was incubated in renatured buffer containing 25 mM Tris-HCl pH 7.5, 1 mM DTT, 5 mM NaF and 0.1 mM Na<sub>3</sub>VO<sub>4</sub> at 4°C for three stages, 1 h, 12 h and 1 h. Next, the gel was incubated in kinase reaction buffer (40 mM HEPES-KOH pH 7.5, 1 mM DTT, 12 mM MgCl<sub>2</sub>, 0.1 mM Na<sub>3</sub>VO<sub>4</sub> and 2 mM EGTA) at 22°C for 30 min, and then incubated in new kinase reaction buffer supplemented with 70 μCi [ $\gamma$ -<sup>32</sup>P] ATP and 9 μl 1 mM cold ATP at 22°C for 1.5 h. The gel was washed five times by 5% [w/v] TCA and 1% [w/v] sodium pyrophosphate for 30 min each. The signal was detected by Typhoon 9410 imager.

### **Electrophysiological assays**

The electrophysiological assays were performed as described (Xu *et al.*, 2006). The cDNA sequence of *OST1* was fused upstream of *YFP<sup>N</sup>*, and the sequence of *AtANN1* or *AtANN1<sup>S289A</sup>* was fused upstream of *YFP<sup>C</sup>* in the *pGEMHE* vector (Geiger *et al.*, 2009; Hua *et al.*, 2012). The cRNAs of *AtANN1-YFP<sup>C</sup>*, *AtANN1<sup>S289A</sup>-YFP<sup>C</sup>* and *OST1-YFP<sup>N</sup>* were transcribed *in vitro* using the T<sub>7</sub> RiboMAX Large Scale RNA Production System (Promega). The oocytes were injected with distilled water (40 nL, as a control), *AtANN1* cRNA (20 ng in 40 nL), *AtANN1<sup>S289A</sup>* cRNA (20 ng in 40 nL), *OST1* cRNA (20 ng in 40 nL), *AtANN1* and *OST1* cRNA mixture (10:10 ng in 40 nL), *AtANN1<sup>S289A</sup>* and *OST1* cRNA mixture (10:10 ng in 40 nL). Then, the injected oocytes were incubated in ND 96 solution containing 96 mM NaCl, 2 mM KCl, 1 mM MgCl<sub>2</sub>, 5 mM HEPES-KOH pH 7.5 and 1.8 mM CaCl<sub>2</sub>, and supplemented with 0.05 mg/mL gentamycin and 0.1 mg/mL streptomycin at 17°C for 2 d.

The two-electrode voltage-clamp technique was performed with a Gene-Clamp 500B amplifier (Axon Instruments) at 22°C. The microelectrodes were filled with 3 M KCl. The bath solution contained 2 mM NaCl, 1 mM KCl, 6 mM MgCl<sub>2</sub>, 185 mM mannitol, 10 mM MES-Tris pH5.5, supplemented with 30 mM BaCl<sub>2</sub> (or CaCl<sub>2</sub>) before recording. The currents were digitized through a Digidata 1322A AC/DC converter with Clampex 9.0 software (Axon Instruments).

### **Mass spectrometry assays**

To identify the putative phosphorylation site of AtANN1 by OST1 *in vitro*, 1 µg His-OST1 and 10 µg GST-AtANN1 purified proteins were incubated in 20 µL of protein kinase reaction buffer containing 20 mM MgCl<sub>2</sub>, 50 mM Tris-HCl pH 7.5, 1 mM DTT and 50 µM ATP, at 30°C for 30 min. The reaction products were reduced by DTT and alkylated by IAM (Iodoacetamide), followed by digestion with trypsin (pH 8.5) at 37°C for 12 h. The results were analyzed by LC-MS/MS as described (Liu *et al.*, 2017).

For LC-MS/MS analysis *in vivo*, total proteins were extracted from 12-d-old

*AtANN1-Myc* overexpressing line treated at 4°C for 10, 30 and 120 min. Protein digestion was performed using filter-aided sample preparation (FASP) method with modifications (Wisniewski *et al.*, 2009). Briefly, 100 µg proteins were dissolved with 50 mM ABC (NH<sub>4</sub>HCO<sub>3</sub>) solution, reduced by DTT at 56°C for 45 min and alkylated by IAM (Iodoacetamide) at 22°C for 30 min in the dark. The solution was transferred into a 10 K ultrafiltration tube (Vivacon 500, Sartorius), spinned at 14,000 g for 20 min with a new collection tube to collect digested peptides. The ABC solution was added into the ultrafiltration tube, and the digested peptide was washed into the collection tube. Phosphopeptides were enriched for LC-MS/MS analysis.

### **Microscale Thermophoresis (MST) assays**

The microscale thermophoresis assays were performed as described (Entzian & Schubert, 2016; Ma *et al.*, 2019). Briefly, the recombinant proteins were purified and replaced with PBST buffer (PBS, 0.005% Tween-20, pH7.4) using column A (Nano Temper Technologies). Then, 110 µL of 10 µM purified recombinant protein GST-AtANN1, GST-AtANN1<sup>S289A</sup>, GST-AtANN1<sup>S289E</sup> or GST was labeled with 6 µL NHS NT-647 dye in the dark for 30 min at room temperature. The labeled protein was collected by column B (Nano Temper Technologies) which was re-equilibrated with HEPES buffer I (20 mM HEPES, 150 mM KCl, 0.5 mg/mL BSA, pH7.4). The initial concentration of CaCl<sub>2</sub> was 2 mM, and then was serially diluted with HEPES buffer II (20 mM HEPES, 150 mM KCl, pH7.4). Finally, the serially diluted CaCl<sub>2</sub> solution was mixed with 10 µL labeled protein. Samples were loaded into capillaries (Nano Temper Technologies) for analysis. The assays were performed with 20% LED power and 20% MST power. Signal thermophoresis and T-jump data were used for calculating dissociation constant (K<sub>d</sub>).

### **Data availability**



The mass spectrometry proteomics data have been deposited to the ProteomeXchange Consortium via the PRIDE partner repository (<https://www.ebi.ac.uk/pride/>) with the dataset identifier PXD022035.



## **Acknowledgements**

We thank Dr. Zhen Li for helping with the LC-MS/MS analysis, and Dr. Adeeba Dark for technical support of aequorin lines. This work was supported by the grants from National Natural Science Foundation of China (31920103002 and 31921001), the Ministry of Agriculture of China for Transgenic Research (2016ZX08009003), the Biotechnology and Biological Sciences Research Council for funding (BB/K009869/1), and Beijing Outstanding University Discipline Program.

## **Author contributions**

SY directed the project. QL and SY designed the experiments. QL performed the experiments with the help of YD, YS, LM, YW and  W. QL, YD, CS, JMD, HK, MRK, ZG, YG, and SY discussed and interpreted the data. QL and YD dra the manuscript. JMD, HK, MRK and SY revised the manuscript.

## **Conflict of interest**

The authors declare that they have no conflict of interest.

## References

- Belin C, de Franco PO, Bourbousse C, Chaignepain S, Schmitter JM, Vavasseur A, Giraudat J, Barbier-Brygoo H, Thomine S (2006) Identification of features regulating OST1 kinase activity and OST1 function in guard cells. *Plant Physiol* 141: 1316-1327
- Breton G, Vazquez-Tello A, Danyluk J, Sarhan F (2000) Two novel intrinsic annexins accumulate in wheat membranes in response to low temperature. *Plant Cell Physiol* 41: 177-184
- Cantero A, Barthakur S, Bushart TJ, Chou S, Morgan RO, Fernandez MP, Clark GB, Roux SJ (2006) Expression profiling of the *Arabidopsis* annexin gene family during germination, de-etiolation and abiotic stress. *Plant Physiol Biochem* 44: 13-24
- Costa-Broseta A, Perea-Resa C, Castillo MC, Ruiz MF, Salinas J, Leon J (2018) Nitric oxide controls constitutive freezing tolerance in *Arabidopsis* by attenuating the levels of osmoprotectants, stress-related hormones and anthocyanins. *Sci Rep* 8: 9268
- Ding Y, Jia Y, Shi Y, Zhang X, Song C, Gong Z, Yang S (2018) OST1-mediated BTF3L phosphorylation positively regulates CBFs during plant cold responses. *EMBO J* 37: e98228
- Ding Y, Li H, Zhang X, Xie Q, Gong Z, Yang S (2015) OST1 kinase modulates freezing tolerance by enhancing ICE1 stability in *Arabidopsis*. *Dev Cell* 32: 278-289
- Ding Y, Lv J, Shi Y, Gao J, Hua J, Song C, Gong Z, Yang S (2019) EGR2 phosphatase regulates OST1 kinase activity and freezing tolerance in *Arabidopsis*. *EMBO J* 38: e99819
- Ding YL, Shi YT, Yang SH (2020) Molecular Regulation of Plant Responses to Environmental

Temperatures. *Mol Plant* 13: 544-564

Dodd AN, Jakobsen MK, Baker AJ, Telzerow A, Hou SW, Laplaze L, Barrot L, Poethig RS, Haseloff J, Webb AAR (2006) Time of day modulates low-temperature Ca<sup>2+</sup> signals in *Arabidopsis*. *Plant J* 48: 962-973

Dodd AN, Kudla J, Sanders D (2010) The language of calcium signaling. *Annu Rev Plant Biol* 61: 593-620

Doherty CJ, Van Buskirk HA, Myers SJ, Thomashow MF (2009) Roles for *Arabidopsis* CAMTA transcription factors in cold-regulated gene expression and freezing tolerance. *Plant Cell* 21: 972-984

Edel KH, Marchadier E, Brownlee C, Kudla J, Hetherington AM (2017) The evolution of calcium-based signalling in plants. *Curr Biol* 27: R667-R679

Entzian C, Schubert T (2016) Studying small molecule-aptamer interactions using MicroScale Thermophoresis (MST). *Methods* 97: 27-34

Finka A, Cuendet AFH, Maathuis FJM, Saidi Y, Goloubinoff P (2012) Plasma membrane cyclic nucleotide gated calcium channels control land plant thermal sensing and acquired thermotolerance. *Plant Cell* 24: 3333-3348

Finn BE, Forsen S (1995) The evolving model of calmodulin structure, function and activation. *Structure* 3: 7-11

Furihata T, Maruyama K, Fujita Y, Umezawa T, Yoshida R, Shinozaki K, Yamaguchi-Shinozaki K (2006) Abscisic acid-dependent multisite phosphorylation regulates the activity of a transcription activator AREB1. *Proc Natl Acad Sci U S A* 103: 1988-1993

Geiger D, Scherzer S, Mumm P, Stange A, Marten I, Bauer H, Ache P, Matschi S, Liese A,

- Al-Rasheid KA, Romeis T, Hedrich R (2009) Activity of guard cell anion channel SLAC1 is controlled by drought-stress signaling kinase-phosphatase pair. *Proc Natl Acad Sci U S A* 106: 21425-21430
- Gorecka KM, Konopka-Postupolska D, Hennig J, Buchet R, Pikula S (2005) Peroxidase activity of annexin 1 from *Arabidopsis thaliana*. *Biochem Biophys Res Commun* 336: 868-875
- Guo XY, Liu DF, Chong K (2018) Cold signaling in plants: Insights into mechanisms and regulation. *J Integr Plant Biol* 60: 745-756
- Hamilton DWA, Hills A, Kohler B, Blatt MR (2000) Ca<sup>2+</sup> channels at the plasma membrane of stomatal guard cells are activated by hyperpolarization and abscisic acid. *Proc Natl Acad Sci USA* 97: 4967-4972
- Hua D, Wang C, He J, Liao H, Duan Y, Zhu Z, Guo Y, Chen Z, Gong Z (2012) A plasma membrane receptor kinase, GHR1, mediates abscisic acid- and hydrogen peroxide-regulated stomatal movement in *Arabidopsis*. *Plant Cell* 24: 2546-2561
- Huh SM, Noh EK, Kim HG, Jeon BW, Bae K, Hu HC, Kwak JM, Park OK (2010) Arabidopsis annexins AnnAt1 and AnnAt4 interact with each other and regulate drought and salt stress responses. *Plant Cell Physiol* 51: 1499-1514
- Jia Y, Ding Y, Shi Y, Zhang X, Gong Z, Yang S (2016) The *cbfs* triple mutants reveal the essential functions of CBFs in cold acclimation and allow the definition of CBF regulons in *Arabidopsis*. *New Phytol* 212: 345-353
- Jiang ZH, Zhou XP, Tao M, Yuan F, Liu LL, Wu FH, Wu XM, Xiang Y, Niu Y, Liu F, Li CJ, Ye R, Byeon B, Xue Y, Zhao HY, Wang HN, Crawford BM, Johnson DM, Hu CX, Pei C et al.

- (2019) Plant cell-surface GIPC sphingolipids sense salt to trigger Ca<sup>2+</sup> influx. *Nature* 572: 341-346
- Kidokoro S, Yoneda K, Takasaki H, Takahashi F, Shinozaki K, Yamaguchi-Shinozaki K (2017) Different cold-signaling pathways function in the responses to rapid and gradual decreases in temperature. *Plant Cell* 29: 760-774
- Kim KN, Cheong YH, Grant JJ, Pandey GK, Luan S (2003) CIPK3, a calcium sensor-associated protein kinase that regulates abscisic acid and cold signal transduction in *Arabidopsis*. *Plant Cell* 15: 411-423
- Kim Y, Park S, Gilmour SJ, Thomashow MF (2013) Roles of CAMTA transcription factors and salicylic acid in configuring the low-temperature transcriptome and freezing tolerance of *Arabidopsis*. *Plant J* 75: 364-376
- Knight H, Trewavas AJ, Knight MR (1996) Cold calcium signaling in *Arabidopsis* involves two cellular pools and a change in calcium signature after acclimation. *Plant Cell* 8: 489-503
- Knight MR (2002) Signal transduction leading to low-temperature tolerance in *Arabidopsis thaliana*. *Philos Trans R Soc Lond B Biol Sci* 357: 871-875
- Knight MR, Campbell AK, Smith SM, Trewavas AJ (1991) Transgenic plant aequorin reports the effects of touch and cold-shock and elicitors on cytoplasmic calcium. *Nature* 352: 524-526
- Konopka-Postupolska D, Clark G, Hofmann A (2011) Structure, function and membrane interactions of plant annexins: An update. *Plant Sci* 181: 230-241
- Kudla J, Becker D, Grill E, Hedrich R, Hippler M, Kummer U, Parniske M, Romeis T,

- Schumacher K (2018) Advances and current challenges in calcium signaling. *New Phytol* 218: 414-431
- Laohavisit A, Davies JM (2011) Annexins. *New Phytol* 189: 40-53
- Laohavisit A, Mortimer JC, Demidchik V, Coxon KM, Stancombe MA, Macpherson N, Brownlee C, Hofmann A, Webb AAR, Miedema H, Battey NH, Davies JM (2009) *Zea mays* annexins modulate cytosolic free Ca<sup>2+</sup> and generate a Ca<sup>2+</sup>-permeable conductance. *Plant Cell* 21: 479-493
- Laohavisit A, Shang ZL, Rubio L, Cui TA, Very AA, Wang AH, Mortimer JC, Macpherson N, Coxon KM, Battey NH, Brownlee C, Park OK, Sentenac H, Shabala S, Webb AAR, Davies JM (2012) Arabidopsis annexin1 mediates the radical-activated plasma membrane Ca<sup>2+</sup>- and K<sup>+</sup>-permeable conductance in root cells. *Plant Cell* 24: 1522-1533
- Lee S, Lee EJ, Yang EJ, Lee JE, Park AR, Song WH, Park OK (2004) Proteomic identification of annexins, calcium-dependent membrane binding proteins that mediate osmotic stress and abscisic acid signal transduction in Arabidopsis. *Plant Cell* 16: 1378-1391
- Lee SC, Lan WZ, Buchanan BB, Luan S (2009) A protein kinase-phosphatase pair interacts with an ion channel to regulate ABA signaling in plant guard cells. *Proc Natl Acad Sci USA* 106: 21419-21424
- Liao CC, Zheng Y, Guo Y (2017) MYB30 transcription factor regulates oxidative and heat stress responses through ANNEXIN-mediated cytosolic calcium signaling in Arabidopsis. *New Phytol* 216: 163-177
- Lin Z, Li Y, Zhang Z, Liu X, Hsu CC, Du Y, Sang T, Zhu C, Wang Y, Satheesh V, Pratibha P,

- Zhao Y, Song CP, Tao WA, Zhu JK, Wang P (2020) A RAF-SnRK2 kinase cascade mediates early osmotic stress signaling in higher plants. *Nat Commun* 11: 613
- Liu HT, Gao F, Li GL, Han JL, Liu DL, Sun DY, Zhou RG (2008) The calmodulin-binding protein kinase 3 is part of heat-shock signal transduction in *Arabidopsis thaliana*. *Plant J* 55: 760-773
- Liu J, Shi Y, Yang S (2018a) Insights into the regulation of CBF cold signaling in plants. *J Integr Plant Biol* 9: 780-795
- Liu Q, Kasuga M, Sakuma Y, Abe H, Miura S, Yamaguchi-Shinozaki K, Shinozaki K (1998) Two transcription factors, DREB1 and DREB2, with an EREBP/AP2 DNA binding domain separate two cellular signal transduction pathways in drought- and low-temperature-responsive gene expression, respectively, in *Arabidopsis*. *Plant Cell* 10: 1391-1406
- Liu Y, Xu C, Zhu Y, Zhang L, Chen T, Zhou F, Chen H, Lin Y (2018b) The calcium-dependent kinase OsCPK24 functions in cold stress responses in rice. *J Integr Plant Biol* 60: 173-188
- Liu Z, Jia Y, Ding Y, Shi Y, Li Z, Guo Y, Gong Z, Yang S (2017) Plasma membrane CRPK1-mediated phosphorylation of 14-3-3 proteins induces their nuclear import to fine-tune CBF signaling during cold response. *Mol Cell* 66: 117-128
- Ma L, Ye JM, Yang YQ, Lin HX, Yue LL, Luo J, Long Y, Fu HQ, Liu XN, Zhang YL, Wang Y, Chen LY, Kudla J, Wang YJ, Han SC, Song CP, Guo Y (2019) The SOS2-SCaBP8 complex generates and fine-tunes an AtANN4-dependent calcium signature under salt stress. *Dev Cell* 48: 697-705

- Ma Y, Dai XY, Xu YY, Luo W, Zheng XM, Zeng DL, Pan YJ, Lin XL, Liu HH, Zhang DJ, Xiao J, Guo XY, Xu SJ, Niu YD, Jin JB, Zhang H, Xu X, Li LG, Wang W, Qian Q et al. (2015) COLD1 confers chilling tolerance in rice. *Cell* 160: 1209-1221
- Ma Y, Szostkiewicz I, Korte A, Moes D, Yang Y, Christmann A, Grill E (2009) Regulators of PP2C phosphatase activity function as abscisic acid sensors. *Science* 324: 1064-1068
- Morgan RO, Martin-Almedina S, Garcia M, Jhoncon-Kooyip J, Fernandez MP (2006) Deciphering function and mechanism of calcium-binding proteins from their evolutionary imprints. *Biochim Biophys Acta* 1763: 1238-1249
- Mori K, Renhu N, Naito M, Nakamura A, Shiba H, Yamamoto T, Suzaki T, Iida H, Miura K (2018) Ca<sup>2+</sup>-permeable mechanosensitive channels MCA1 and MCA2 mediate cold-induced cytosolic Ca<sup>2+</sup> increase and cold tolerance in *Arabidopsis*. *Sci Rep* 8: 550
- Mustilli AC, Merlot S, Vavasseur A, Fenzi F, Giraudat J (2002) Arabidopsis OST1 protein kinase mediates the regulation of stomatal aperture by abscisic acid and acts upstream of reactive oxygen species production. *Plant Cell* 14: 3089-3099
- Park SY, Fung P, Nishimura N, Jensen DR, Fujii H, Zhao Y, Lumba S, Santiago J, Rodrigues A, Chow TF, Alfred SE, Bonetta D, Finkelstein R, Provart NJ, Desveaux D, Rodriguez PL, McCourt P, Zhu JK, Schroeder JI, Volkman BF et al. (2009) Abscisic acid inhibits type 2C protein phosphatases via the PYR/PYL family of START proteins. *Science* 324: 1068-1071
- Pei ZM, Murata Y, Benning G, Thomine S, Klusener B, Allen GJ, Grill E, Schroeder JI (2000) Calcium channels activated by hydrogen peroxide mediate abscisic acid signalling in guard cells. *Nature* 406: 731-734



- Qiao B, Zhang Q, Liu DL, Wang HQ, Yin JY, Wang R, He ML, Cui M, Shang ZL, Wang DK, Zhu ZG (2015) A calcium-binding protein, rice annexin OsANN1, enhances heat stress tolerance by modulating the production of H<sub>2</sub>O<sub>2</sub>. *J Exp Bot* 66: 5853-5866
- Reddy ASN, Ali GS, Celesnik H, Day IS (2011) Coping with stresses: Roles of calcium- and calcium/calmodulin-regulated gene expression. *Plant Cell* 23: 2010-2032
- Renaut J, Hausman JF, Wisniewski ME (2006) Proteomics and low-temperature studies: bridging the gap between gene expression and metabolism. *Physiol Plant* 126: 97-109
- Rentel MC, Knight MR (2004) Oxidative stress-induced calcium signaling in *Arabidopsis*. *Plant Physiol* 135: 1471-1479
- Richards SL, Laohavisit A, Mortimer JC, Shabala L, Swarbreck SM, Shabala S, Davies JM (2014) Annexin 1 regulates the H<sub>2</sub>O<sub>2</sub>-induced calcium signature in *Arabidopsis thaliana* roots. *Plant J* 77: 136-145
- Sato A, Sato Y, Fukao Y, Fujiwara M, Umezawa T, Shinozaki K, Hibi T, Taniguchi M, Miyake H, Goto DB, Uozumi N (2009) Threonine at position 306 of the KAT1 potassium channel is essential for channel activity and is a target site for ABA-activated SnRK2/OST1/SnRK2.6 protein kinase. *Biochem J* 424: 439-448
- Shi YT, Tian SW, Hou LY, Huang XZ, Zhang XY, Guo HW, Yang SH (2012) Ethylene signaling negatively regulates freezing tolerance by repressing expression of *CBF* and type-A *ARR* genes in *Arabidopsis*. *Plant Cell* 24: 2578-2595
- Short EF, North KA, Roberts MR, Hetherington AM, Shirras AD, McAinsh MR (2012) A stress-specific calcium signature regulating an ozone-responsive gene expression network in *Arabidopsis*. *Plant J* 71: 948-961

- Soma F, Takahashi F, Suzuki T, Shinozaki K, Yamaguchi-Shinozaki K (2020) Plant Raf-like kinases regulate the mRNA population upstream of ABA-unresponsive SnRK2 kinases under drought stress. *Nat Commun* 11: 1373
- Stockinger EJ, Gilmour SJ, Thomashow MF (1997) *Arabidopsis thaliana* CBF1 encodes an AP2 domain-containing transcriptional activator that binds to the C-repeat/DRE, a cis-acting DNA regulatory element that stimulates transcription in response to low temperature and water deficit. *Proc Natl Acad Sci USA* 94: 1035-1040
- Takahashi Y, Zhang JB, Hsu PK, Ceciliato PHO, Zhang L, Dubeaux G, Munemasa S, Ge CN, Zhao YD, Hauser F, Schroeder JI (2020) MAP3Kinase-dependent SnRK2-kinase activation is required for abscisic acid signal transduction and rapid osmotic stress response. *Nat Commun* 11: 12
- Thomashow MF (1999) Plant cold acclimation: Freezing tolerance genes and regulatory mechanisms. *Annu Rev Plant Physiol Plant Mol Biol* 50: 571-599
- Tian W, Hou CC, Ren ZJ, Wang C, Zhao FG, Dahlbeck D, Hu SP, Zhang LY, Niu Q, Li LG, Staskawicz BJ, Luan S (2019) A calmodulin-gated calcium channel links pathogen patterns to plant immunity. *Nature* 572: 131-135
- Ticha M, Richter H, Ovecka M, Maghelli N, Hrbackova M, Dvorak P, Samaj J, Samajova O (2020) Advanced microscopy reveals complex developmental and subcellular localization patterns of ANNEXIN 1 in Arabidopsis. *Front Plant Sci* 11: 1153
- Toyota M, Spencer D, Sawai-Toyota S, Wang JQ, Zhang T, Koo AJ, Howe GA, Gilroy S (2018) Glutamate triggers long-distance, calcium-based plant defense signaling. *Science* 361: 1112-1115

- Tunc-Ozdemir M, Tang C, Ishka MR, Brown E, Groves NR, Myers CT, Rato C, Poulsen LR, McDowell S, Miller G, Mittler R, Harper JF (2013) A cyclic nucleotide-gated channel (CNGC16) in pollen is critical for stress tolerance in pollen reproductive development. *Plant Physiol* 161: 1010-1020
- Viridi AS, Singh S, Singh P (2015) Abiotic stress responses in plants: roles of calmodulin-regulated proteins. *Front Plant Sci* 6: 809
- Wang X, Ding Y, Li Z, Shi Y, Wang J, Hua J, Gong Z, Zhou JM, Yang S (2019) PUB25 and PUB26 promote plant freezing tolerance by degrading the cold signaling negative regulator MYB15. *Dev Cell* 51: 222-235
- Wang X, Ma XL, Wang H, Li BJ, Clark G, Guo Y, Roux S, Sun DY, Tang WQ (2015) Proteomic study of microsomal proteins reveals a key role for Arabidopsis Annexin 1 in mediating heat stress-induced increase in intracellular calcium levels. *Mol Cell Proteomics* 14: 686-694
- Ward JM, Maser P, Schroeder JI (2009) Plant ion channels: gene families, physiology, and functional genomics analyses. *Annu Rev Physiol* 71: 59-82
- Wisniewski JR, Zougman A, Nagaraj N, Mann M (2009) Universal sample preparation method for proteome analysis. *Nat Methods* 6: 359-362
- Xu J, Li H-D, Chen L-Q, Wang Y, Liu L-L, He L, Wu W-H (2006) A protein kinase, interacting with two calcineurin B-like proteins, regulates K<sup>+</sup> transporter AKT1 in *Arabidopsis*. *Cell* 125: 1347-1360
- Yu X, Xu GY, Li B, Vespoli LD, Liu H, Moeder W, Chen SX, de Oliveira MVV, de Souza SA, Shao WY, Rodrigues B, Ma Y, Chhajed S, Xue SW, Berkowitz GA, Yoshioka K, He P,

- Shan LB (2019) The receptor kinases BAK1/SERK4 regulate Ca<sup>2+</sup> channel-mediated cellular homeostasis for cell death containment. *Curr Biol* 29: 3778-3790
- Zhang D, Guo X, Xu Y, Li H, Ma L, Yao X, Weng Y, Guo Y, Liu CM, Chong K (2019) OsCIPK7 point-mutation leads to conformation and kinase-activity change for sensing cold response. *J Integr Plant Biol* 61: 1194-1200
- Zhang W, Fan LM, Wu WH (2007) Osmo-sensitive and stretch-activated calcium-permeable channels in *Vicia faba* guard cells are regulated by actin dynamics. *Plant Physiol* 143: 1140-1151
- Zhao CZ, Zhang ZJ, Xie SJ, Si T, Li YY, Zhu JK (2016) Mutational evidence for the critical role of CBF transcription factors in cold acclimation in *Arabidopsis*. *Plant Physiol* 171: 2744-2759
- Zhu JK (2016) Abiotic stress signaling and responses in plants. *Cell* 167: 313-324

## FIGURE LEGENDS

### **Figure 1. AtANN1 mediates plants response to freezing tolerance in CBF-dependent manner.**

A–C Freezing phenotype (A), survival rate (B), and ion leakage (C) of Col-0, *atann1*, and *atann1 AtANN1* (#10) plants. Twelve-day-old plants grown on MS medium at 22°C were exposed to freezing temperatures (NA for non-acclimation, –5°C, 30 min; CA for cold acclimation, –8°C, 40 min). Representative pictures are shown in (A).

D,E Expression of *CBFs* (D) and their targets (E) in Col-0, *atann1*, and *atann1 AtANN1* (#10) plants. Twelve-day-old plants grown on MS medium at 22°C were placed at 4°C for 3 h (D) or 24 h (E), and total RNA was extracted and subjected to qRT-PCR analysis. Relative transcript levels in untreated Col-0 plants were set to 1.

Data information: In (B and C), the data represent means  $\pm$  SE of three independent experiments, each with three technical repeats (n=25 seedlings for each repeat). \*\**P* < 0.01, two-tailed *t*-test. In (D and E), the data represent means  $\pm$  SD of three technical replicates (\*\**P* < 0.01, \* *P* < 0.05, two-tailed *t*-test). Three independent experiments showed a similar result.

### **Figure 2. OST1 interacts with the Ca<sup>2+</sup>-permeable transporter AtANN1.**

A Time-course analysis of cytosolic free calcium concentration ( $[Ca^{2+}]_{cyt}$ ) dynamics in 10-d-old wild type (Col-0), *atann1*, and *atann1 AtANN1* complementation line (#10) after treatment with ice-cold water or ice-cold water containing 10 mM LaCl<sub>3</sub> (arrow shows the time point of treatment). Luminescence was recorded at 1-s intervals.

B Quantification of the cold-induced  $[Ca^{2+}]_{cyt}$  changes shown in (A). Peak  $[Ca^{2+}]_{cyt}$  indicates the highest  $[Ca^{2+}]_{cyt}$  after treatment.

C GST pull-down assay showing that OST1 interacts with AtANN1 *in vitro*. Purified recombinant GST-OST1, GST-OST1<sup>G33R</sup>, or GST proteins from *E. coli* were immunoprecipitated with GST beads and then incubated with MBP-His-AtANN1. Precipitated proteins were detected with anti-GST and anti-His antibodies.

D Interaction of OST1 and AtANN1 detected by bimolecular fluorescence complementation (BiFC) assays. The construct combinations were co-transformed into *N. benthamiana* leaves and expressed for 2 d. The signal was detected by confocal microscopy. Scale bar, 25  $\mu$ m. The fluorescence intensity was scanned using the ImageJ plot profile tool. The y-axes indicate relative pixel intensity.

E,F Interaction of OST1 and AtANN1 detected by Co-IP assays in *Arabidopsis*. Twelve-day-old *OST1-Myc* overexpressing plants grown on MS medium at 22°C were placed at 4°C for 0, 0.5, 2 h, and total proteins were extracted and immunoprecipitated with anti-Myc agarose beads. The wild type (Col-0) treated with 4°C for 2 h was used as control. The OST1-Myc protein was detected with anti-Myc antibody and the AtANN1 protein was detected with anti-AtANN1 antibody. Representative pictures are shown in (E) and relative protein level in (F).

G Co-IP assay showing the interaction between OST1 and AtANN1 *in vivo*. The construct combinations were expressed in *N. benthamiana* leaves. Total proteins were extracted after the *N. benthamiana* leaves treated with 4°C or 22°C and immunoprecipitated with anti-Myc agarose beads. The proteins were detected with anti-Myc and anti-GFP antibodies.

Data information: In (A and B), the data represent means  $\pm$  SD of 20 seedlings. Three independent experiments showed a similar result. In (F), the data represent means  $\pm$  SD of three technical replicates. Different letters represent significant difference at  $P < 0.05$  (one-way ANOVA). In (C-G), representative data were shown, and at least three independent experiments showed a similar result.

**Figure 3. Genetic analysis of *OST1* and *AtANN1*.**

A–C Freezing phenotype (A), survival rate (B) and ion leakage (C) of Col-0, *ost1-3*, *atann1*, and *atann1 ost1-3*. Twelve-day-old plants grown on MS medium at 22°C were exposed to freezing temperatures (NA, –5°C, 30 min; CA, –8°C, 40 min). Representative pictures are shown in (A).

D,E *OST1* gene expression (D) and protein levels of OST1 and AtANN1 (E) in Col-0,

*OST1-Myc*, *atann1* and *OST1-Myc atann1*. OST1 and AtANN1 proteins were detected with anti-Myc and anti-AtANN1 antibodies. HSP90 was used as a control.

F–H Freezing phenotype (F), survival rate (G), and ion leakage (H) of Col-0, *OST1-Myc*, *atann1* and *OST1-Myc atann1*. 12-d-old plants grown on MS medium at 22°C were exposed to freezing temperatures (NA, -5°C, 30 min; CA, -8°C, 40 min). Representative pictures are shown in (F).

Data information: In (B, C, G and H), the data represent means  $\pm$  SE of three independent experiments, each with three technical repeats (n=19 seedlings for each repeat). Different letters represent significant difference at  $P < 0.05$  (one-way ANOVA). In (D), the data represent means  $\pm$  SD of three technical replicates.

**Figure 4. AtANN1 is phosphorylated by OST1 at S289.**

A,B OST1 phosphorylates AtANN1 (A) and AtANN4 (B) *in vitro*. Purified recombinant MBP-His-OST1 was incubated with GST-AtANN1, GST-AtANN4 or GST in kinase reaction buffer with 1  $\mu$ Ci [ $\gamma$ -<sup>32</sup>P] ATP for 30 min at 30°C, followed by separation with SDS-PAGE. Phosphorylated AtANN1 and AtANN4 were detected by autoradiography. Recombinant OST1, AtANN1 and AtANN4 were stained by Coomassie brilliant blue (CBB).

C In-gel kinase assays of OST1 in Col-0 and *ost1-3* mutant under cold stress. Twelve-day-old Col-0 and *ost1-3* mutant were treated at 4°C for 2 h. Total protein extracts were prepared and separated on a SDS-PAGE gel containing 0.2 mg/mL GST-AtANN1 as a substrate, and incubated with 70  $\mu$ Ci [ $\gamma$ -<sup>32</sup>P] ATP. Top, autoradiograph; bottom, CBB staining.

D *In vitro* kinase analysis of the indicated mutant forms of AtANN1 by OST1. After phosphorylation, the proteins were separated by SDS-PAGE and subjected to autoradiography. Top, autoradiograph; bottom, CBB staining.

E OST1 phosphorylates AtANN1 at S289 *in vivo* in LC/MS analysis. Total proteins were extracted from 12-d-old *AtANN1-Myc* overexpressing plants treated at 4°C for 0, 10, 30 and 120 min, followed by trypsin digestion. Phosphopeptides were enriched for mass spectrometry analysis. Representative picture for 10 min was shown.

Data information: In (A–C), representative data were shown, and three independent experiments showed a similar result.

**Figure 5. The phosphorylation of AtANN1 by OST1 is required for plant freezing tolerance**

A–C Freezing phenotype (A), survival rate (B), and ion leakage (C) of Col-0, *atann1*, and *atann1 AtANN1<sup>S289E</sup>* (#5) plants. 12-d-old plants grown on MS medium at 22°C were exposed to freezing temperatures (NA, –5°C, 30 min; CA, –8°C, 40 min). Representative pictures are shown in (A).

D–F Freezing phenotype (D), survival rate (E), and ion leakage (F) of Col-0, *Atann1*, and *atann1 AtANN1<sup>S289A</sup>* (#16) plants. 12-d-old plants grown on MS medium at 22°C were exposed to freezing temperatures (NA, –5°C, 30 min; CA, –8°C, 40 min). Representative pictures are shown in (D).

Data information: In (B, C, E and F), the data represent means ± SE of three independent experiments, each with three technical repeats (n=25 seedlings for each repeat). \*\**P* < 0.01, two-tailed *t*-test.

**Figure 6. The Ca<sup>2+</sup> transport activity of AtANN1 is enhanced by OST1.**

A AtANN1 current recordings in *Xenopus* oocytes. Whole-cell currents were recorded in *Xenopus* oocytes injected with ddH<sub>2</sub>O or with *AtANN1*, *OST1*, or *AtANN1* + *OST1* cRNA. Bath solution was described in Materials and Methods. The voltage protocol as well as time and current scale bars for the recordings are shown.

B Current-voltage (*I*–*V*) relationship of the steady-state whole-cell currents in *Xenopus* oocytes described in (A). Negative current is influx of cations into the oocytes.

C Percentage of total *Xenopus* oocytes in different nA range according to (A).

D AtANN1 current recordings in oocytes. Whole-cell currents were recorded in *Xenopus* oocytes injected with ddH<sub>2</sub>O or with *AtANN1*, *AtANN1<sup>S289A</sup>*, *OST1*, *AtANN1* + *OST1*, and *AtANN1<sup>S289A</sup>* + *OST1* cRNA.

E Current-voltage (*I*–*V*) relationship of the steady-state whole-cell currents in



*Xenopus* oocytes described in (D).

F Percentage of total *Xenopus* oocytes in different nA range according to (D).

Data information: In (A and D), representative data were shown. In (B and E), the data represent means  $\pm$  SD of 5 oocytes. Three independent experiments showed a similar result.

**Figure 7. Phosphorylation of AtANN1 by OST1 promotes its Ca<sup>2+</sup>-binding activity.**

A Time-course analysis of [Ca<sup>2+</sup>]<sub>cyt</sub> dynamics between 10-day-old wild type (Col-0) and *ost1-3* mutant after treatment with ice-cold water or ice-cold water containing 10 mM LaCl<sub>3</sub> (arrow shows the time point of treatment). Luminescence was recorded at 1-s intervals.

B Quantification of the cold-induced [Ca<sup>2+</sup>]<sub>cyt</sub> changes shown in (A). Peak [Ca<sup>2+</sup>]<sub>cyt</sub> indicates the highest [Ca<sup>2+</sup>]<sub>cyt</sub> after treatment.

C MST assays of the calcium-binding affinity of GST-AtANN1, GST-AtANN1<sup>S289A</sup>, and GST-AtANN1<sup>S289E</sup>. GST was used as a control.

D A proposed working model. Under normal conditions, OST1 protein kinase interacts with PP2C, which inhibits the kinase activity of OST1. AtANN1 is localized in the cytosol and at the plasma membrane. Under cold stress, OST1 is activated and phosphorylates AtANN1, which, on the one hand, enhances the Ca<sup>2+</sup> transport activity of AtANN1, and, on the other, promotes the Ca<sup>2+</sup>-binding activity of AtANN1. This dual role of phosphorylation results in increased cold stress-induced [Ca<sup>2+</sup>]<sub>cyt</sub>. Consequently, AtANN1 indirectly facilitates the expression of *CBFs* and *CORs* to positively regulate plant freezing tolerance.

Data information: In (A and B), the data represent means  $\pm$  SD of 20 seedlings (\*\*  $P < 0.01$ , student *t*-test). Three independent experiments showed a similar result. In (C), the data represent means  $\pm$  SD of three biological replicates.

**EXPANDED VIEW FIGURES**

**Figure EV1. AtANN1 and AtANN4 modulate plant freezing tolerance.**

A,B mRNA (A) and the protein (B) levels of AtANN1 in the wild type (Col-0), *atann1* and *atann1 AtANN1* (#4 and #10) seedlings. AtANN1 protein was detected with anti-GFP antibody. HSP90 was used as a control.

C–E Freezing phenotype (C), survival rate (D), and ion leakage (E) of Col-0, *atann1*, and *atann1 AtANN1* (#4) plants. 12-d-old plants grown on MS medium at 22°C were exposed to freezing temperatures (NA for non-acclimation, –5°C, 30 min; CA for cold acclimation, –8°C, 40 min). Representative pictures are shown in (C).

F,G Freezing phenotype (F) and survival rate (G) of Col-0, *atann4-1*, and *atann4-2* plants. 12-d-old plants grown on MS medium at 22°C were exposed to freezing temperatures (NA, –5°C, 30 min; CA, –8°C, 40 min). Representative pictures are shown in (F).

H,I Freezing phenotype (H) and survival rate (I) of Col-0, *atann1*, *atann4-1* and *atann1 atann4-1* plants. 12-d-old plants grown on MS medium at 22°C were exposed to freezing temperatures (NA, –5°C, 30 min; CA, –8°C, 40 min). Representative pictures are shown in (H).

Data information: In (A), the data represent means  $\pm$  SD of three technical replicates. In (D, E, G, and I), the data represent means  $\pm$  SE of three independent experiments, each with three technical repeats (n=25 seedlings for each repeat for D, E, and G, and n=19 for I). In (D, E, and G),  $**P < 0.01$ , two-tailed *t*-test. In (I), different letters represent significant difference at  $P < 0.05$  (one-way ANOVA).

**Figure EV2. Analysis of  $[Ca^{2+}]_{cyt}$  in *atann1* mutant under cold stress.**

A–C Pseudocolor luminescence image of  $Ca^{2+}$ -dependent photons emitted by 10-d-old wild type (Col-0), *atann1*, and *atann1 AtANN1* complementation line (#10) after treatment with ice-cold water (4°C water) (A). Seedlings grown at 22°C or treated with water at room temperature (22°C water) were used as controls. Luminescence signals were collected for 8 min and the color scale indicates photon counts per pixel (A, top), and photos was taken as control (A, bottom). Analysis of relative luminescence signal intensity in (A) was shown (B). Aequorin protein levels of

seedlings used in (A) detected with anti-Aequorin antibody (C). HSP90 was used as a control.

D Time-course analysis of  $[Ca^{2+}]_{cyt}$  dynamics between 10-day-old wild type (Col-0) and *ann1-2* mutant after treatment with 4°C water (arrow shows the time point of treatment). Luminescence was recorded at 1-s intervals. Quantification of the cold-induced  $[Ca^{2+}]_{cyt}$  changes shown in the left. Peak  $[Ca^{2+}]_{cyt}$  indicates the highest  $[Ca^{2+}]_{cyt}$  after treatment.

E Time-course analysis of cytosolic free calcium concentration ( $[Ca^{2+}]_{cyt}$ ) dynamics in 10-d-old wild type (Col-0), *atann1*, and *atann1 AtANN1* complementation line (#10) after treatment with 22°C water or 22°C water containing 10 mM LaCl<sub>3</sub> (arrow shows the time point of treatment). Luminescence was recorded at 1-s intervals.

F Time-course analysis of  $[Ca^{2+}]_{cyt}$  dynamics between 10-day-old wild type (Col-0) and *atann4-1* mutant after treatment with 4°C water (left) or 22°C water (right). Luminescence was recorded at 1-s intervals. Quantification of the cold-induced  $[Ca^{2+}]_{cyt}$  changes shown in the left. Peak  $[Ca^{2+}]_{cyt}$  indicates the highest  $[Ca^{2+}]_{cyt}$  after treatment.

Data information: In (B), the data represent means  $\pm$  SD (n=8). Different letters represent significant difference at  $P < 0.05$  (one-way ANOVA). Three independent experiments showed a similar result. In (D–F), the data represent means  $\pm$  SD (n=15; \*\* $P < 0.01$ , two-tailed  $t$ -test). Three independent experiments showed a similar result.

### **Figure EV3. AtANN1 and AtANN4 interact with OST1.**

A Diagram of AtANN1-truncated proteins used for the yeast two-hybrid assays described in (B).

B The interaction of OST1 and AtANN1 in yeast cells. Yeast cells were grown on SC/–Trp/–Leu (–WL) medium for 2 d or SC/–His/–Trp/–Leu (–HWL) medium supplemented with 2 mM 3-AT for 4 d.

C The protein level of AtANN1 and OST1/OST1<sup>G33R</sup> in BiFC assays described in Figure 2D. OST1-YNE and OST1<sup>G33R</sup>-YNE proteins were detected with anti-Myc antibody. AtANN1-YCE protein was detected with anti-HA antibody.

D GST pull-down assay showing that OST1 interacts with AtANN4 *in vitro*. Purified recombinant GST-AtANN1, GST- AtANN4, or GST proteins from *E. coli* were immunoprecipitated with GST beads and then incubated with MBP-His-OST1.

Precipitated proteins were detected with anti-GST and anti-His antibodies.

E Co-IP assay showing the interaction between OST1 and AtANN4 *in vivo*. The construct combinations were expressed in *N. benthamiana* leaves. Total proteins were extracted and immunoprecipitated with anti-Myc agarose beads. The proteins were detected with anti-Myc and anti-GFP antibodies.

**Figure EV4. The Ca<sup>2+</sup> transport activity of AtANN1 is enhanced by OST1.**

A AtANN1 current recordings in *Xenopus* oocytes. Whole-cell currents were recorded in oocytes with injection of cRNA of ddH<sub>2</sub>O, AtANN1, OST1 and AtANN1 + OST1.

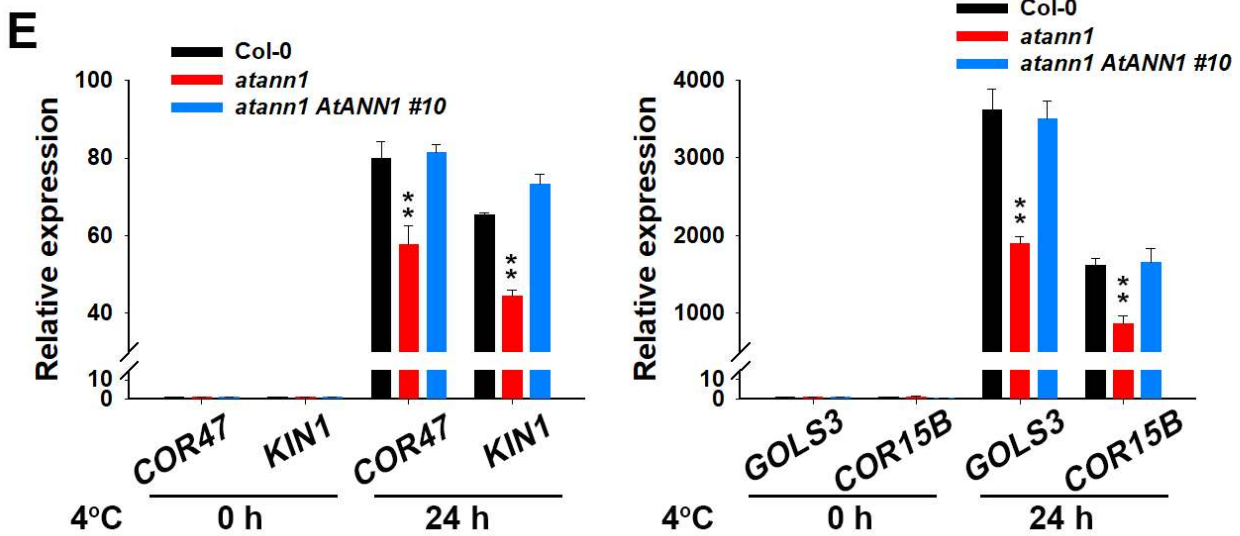
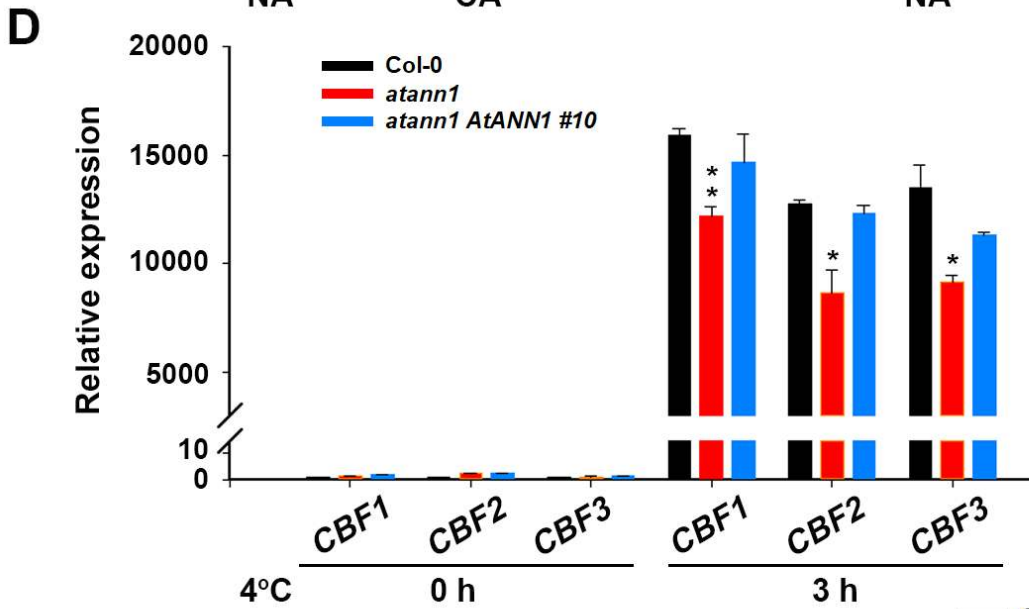
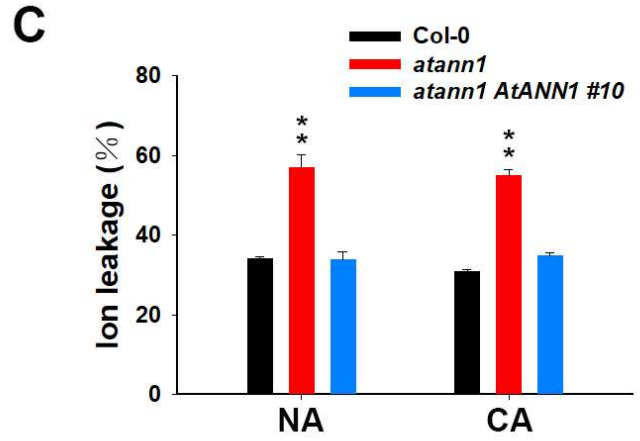
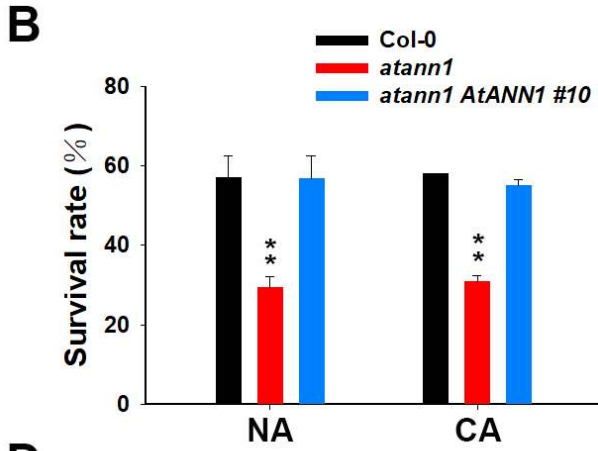
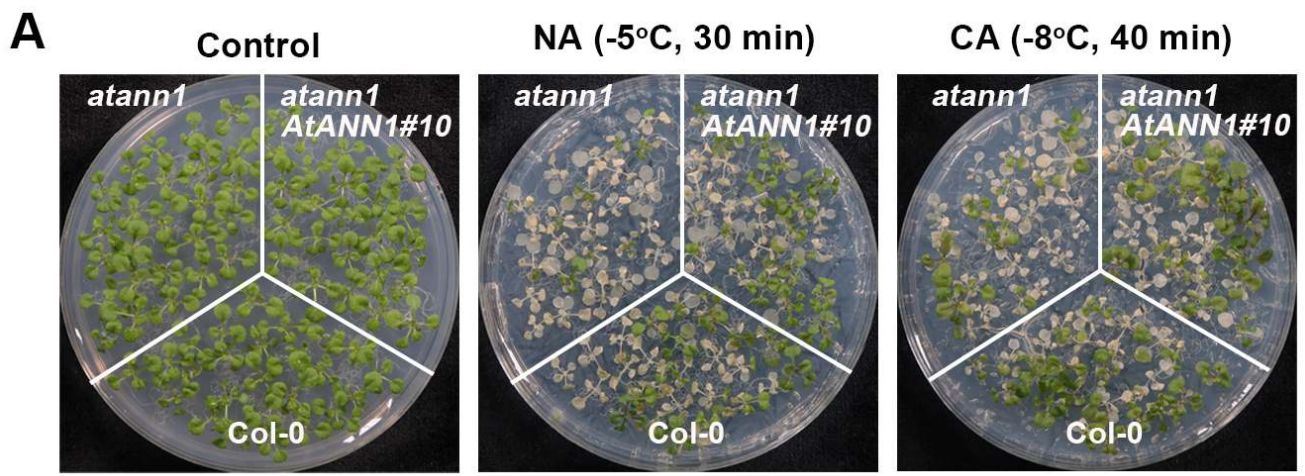
B Current-voltage (*I*-*V*) relationship of the steady-state whole-cell currents in *Xenopus* oocytes described in (A). Negative current is influx of cations into the oocytes.

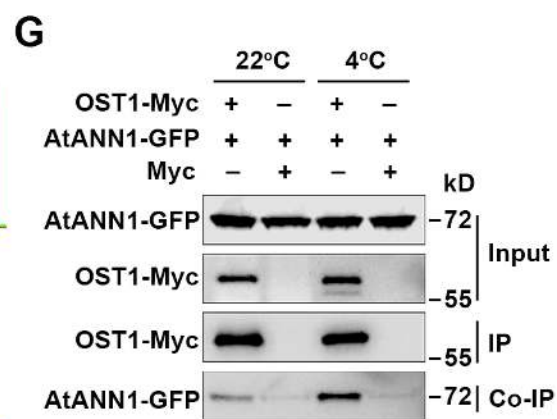
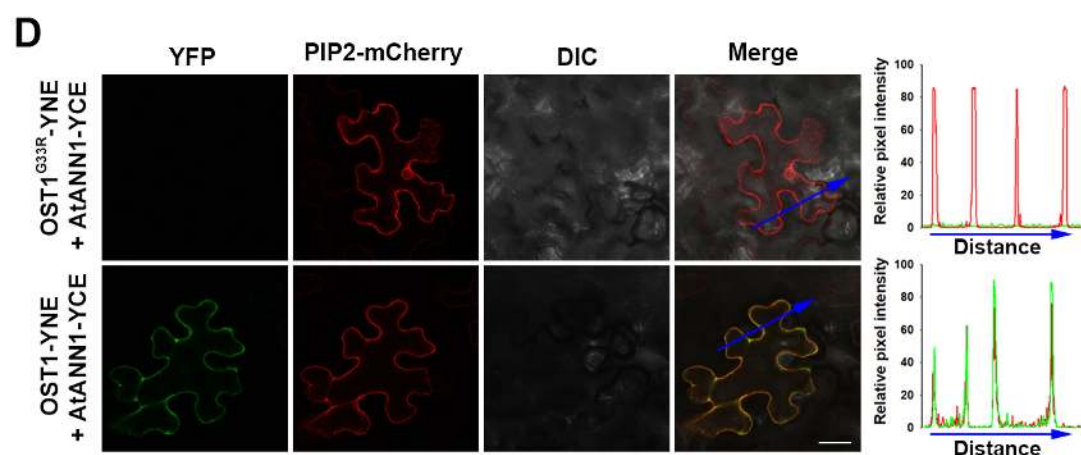
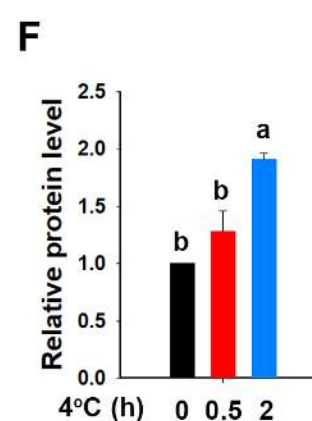
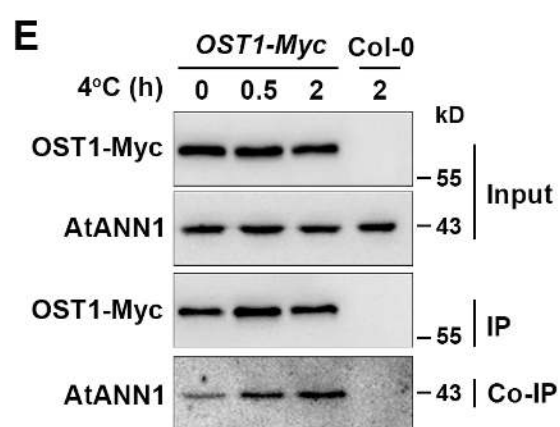
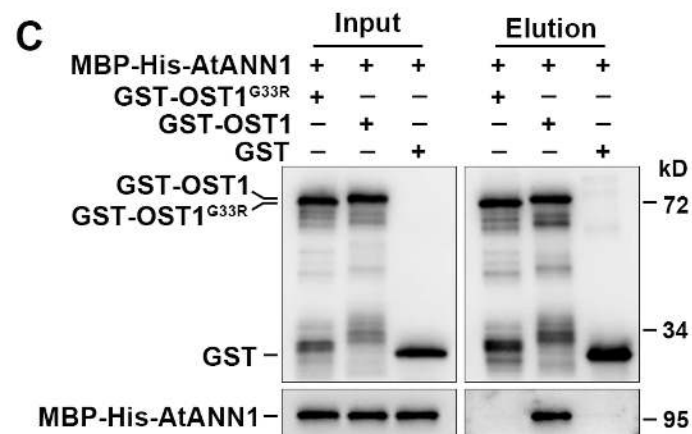
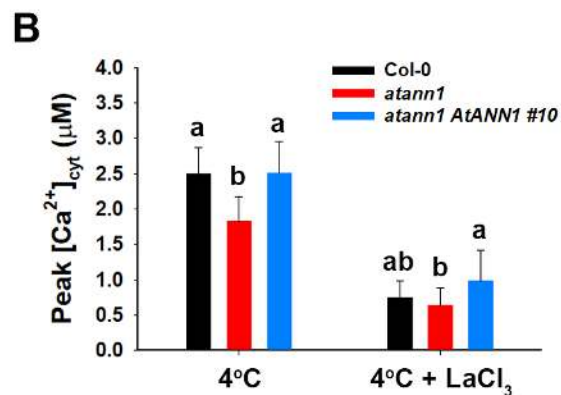
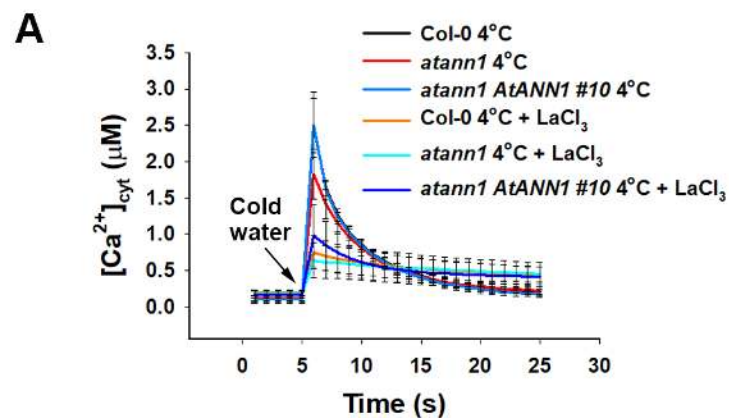
C Percentage of total *Xenopus* oocytes in different nA range according to (A).

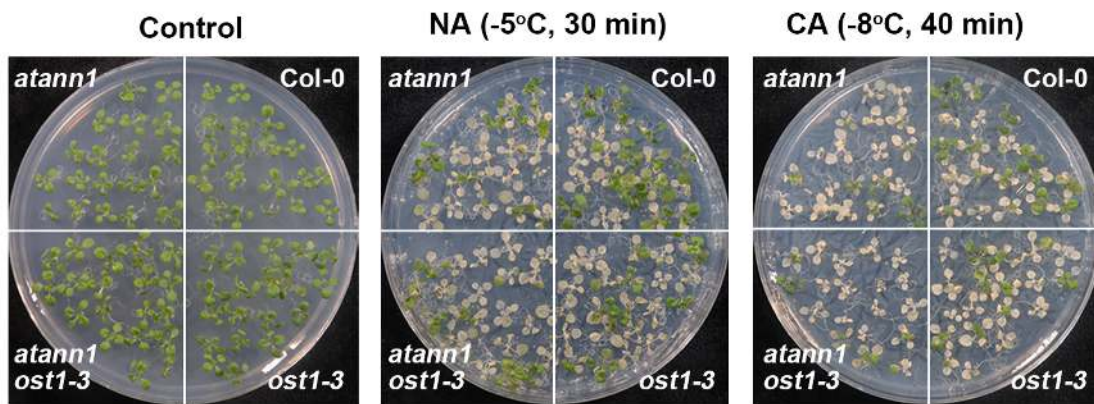
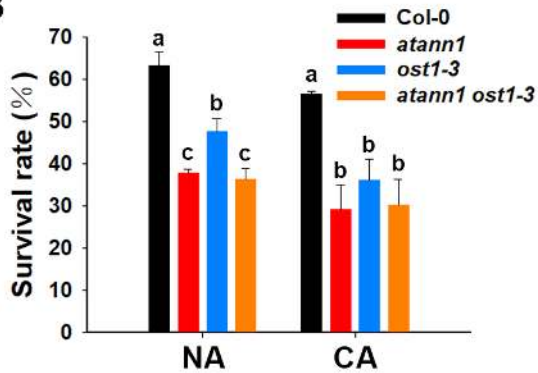
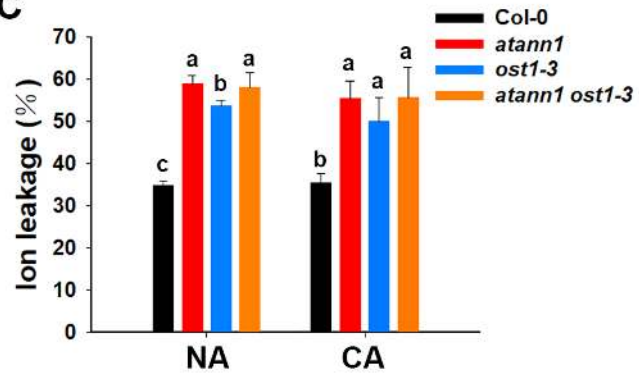
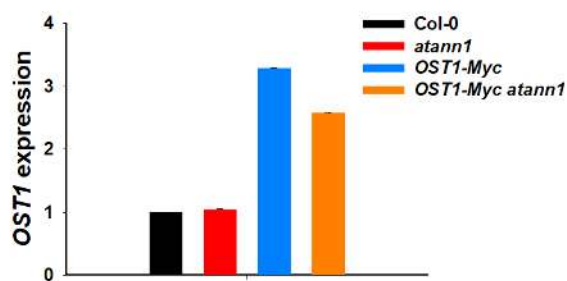
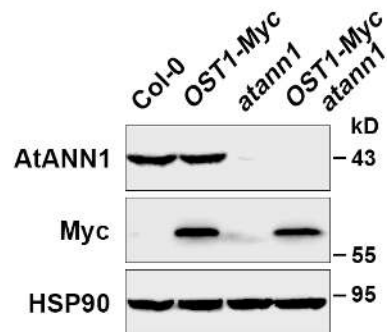
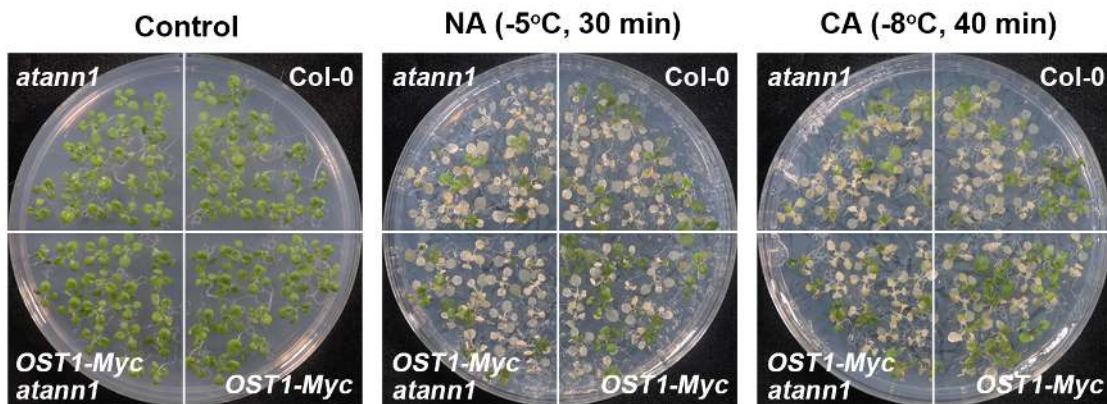
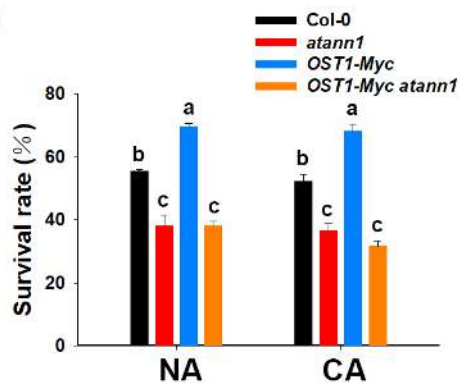
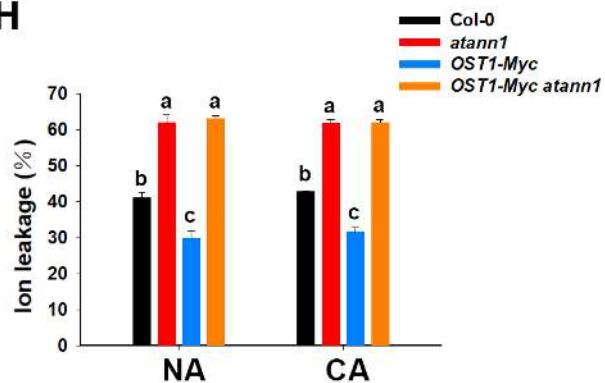
D Time-course analysis of cytosolic free calcium concentration ( $[Ca^{2+}]_{cyt}$ ) dynamics in 10-d-old wild type (Col-0) and *ost1-3* mutant after treatment with 22°C water or 22°C water containing 10 mM LaCl<sub>3</sub> (arrow shows the time point of treatment). Luminescence was recorded at 1-s intervals. Quantification of the cold-induced  $[Ca^{2+}]_{cyt}$  changes shown in the top. Peak  $[Ca^{2+}]_{cyt}$  in the bottom indicates the highest  $[Ca^{2+}]_{cyt}$  after treatment.

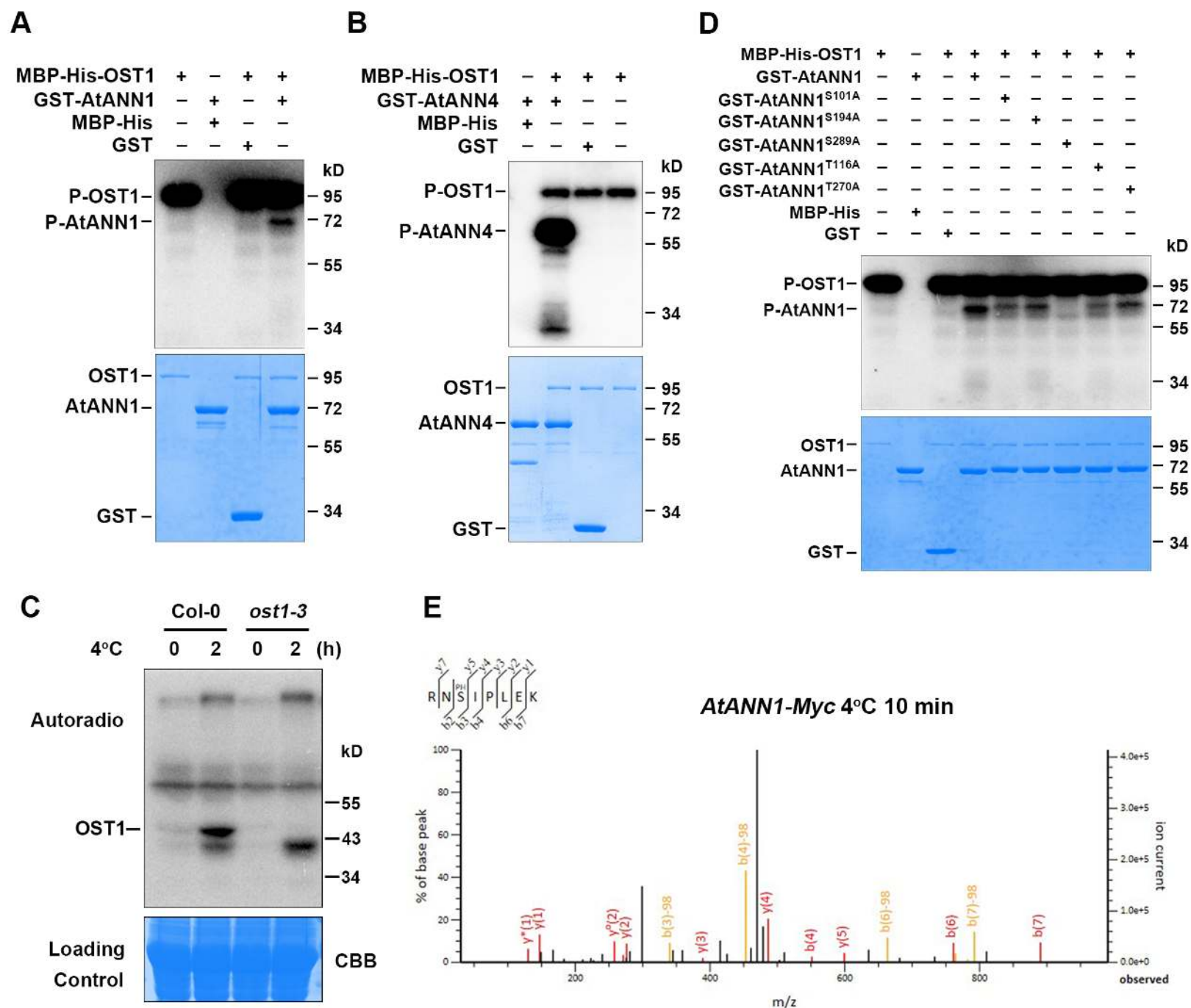
E The protein level of GST, GST-AtANN1, GST-AtANN1<sup>S289A</sup> and GST-AtANN1<sup>S289E</sup> in MST assays described in Figure 7C.

Data information: In (B), the data represent means ± SD of 5 oocytes. Three independent experiments showed a similar result. In (D), the data represent means ± SD of 20 seedlings. Three independent experiments showed a similar result.

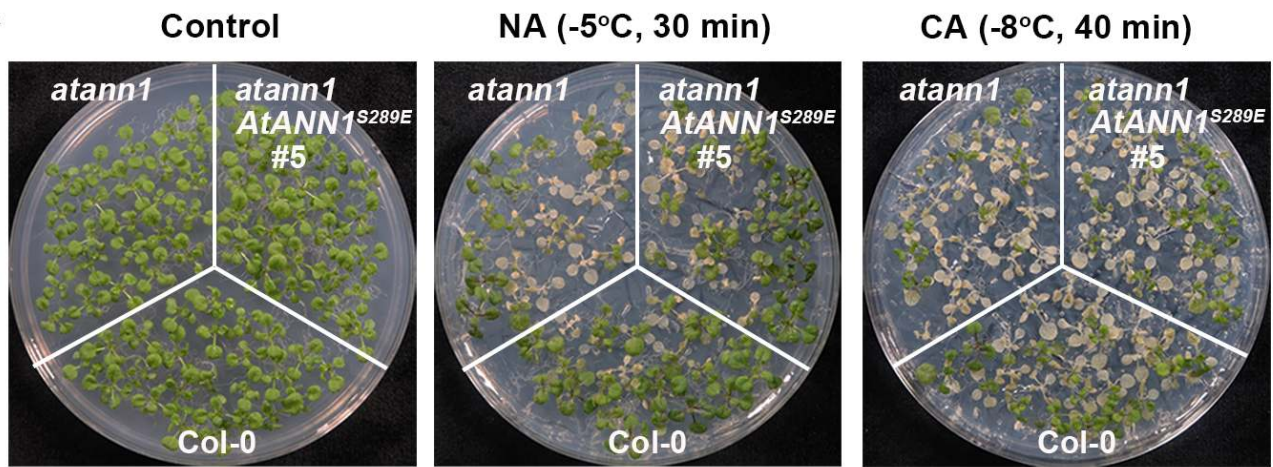
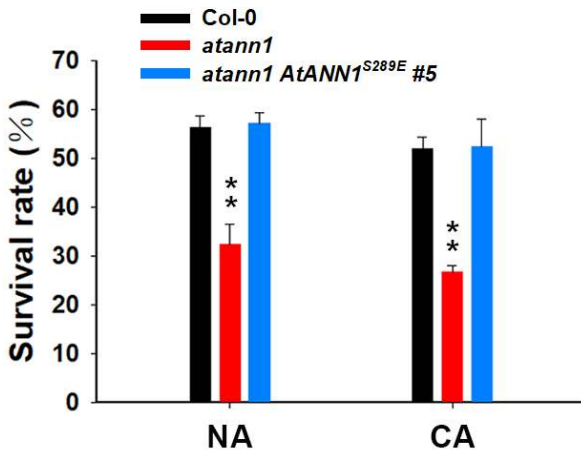
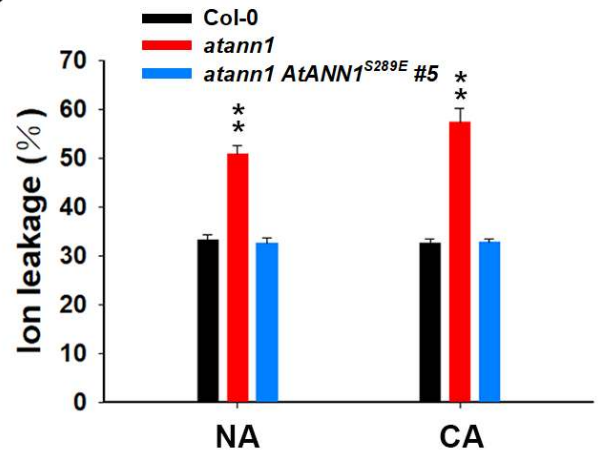
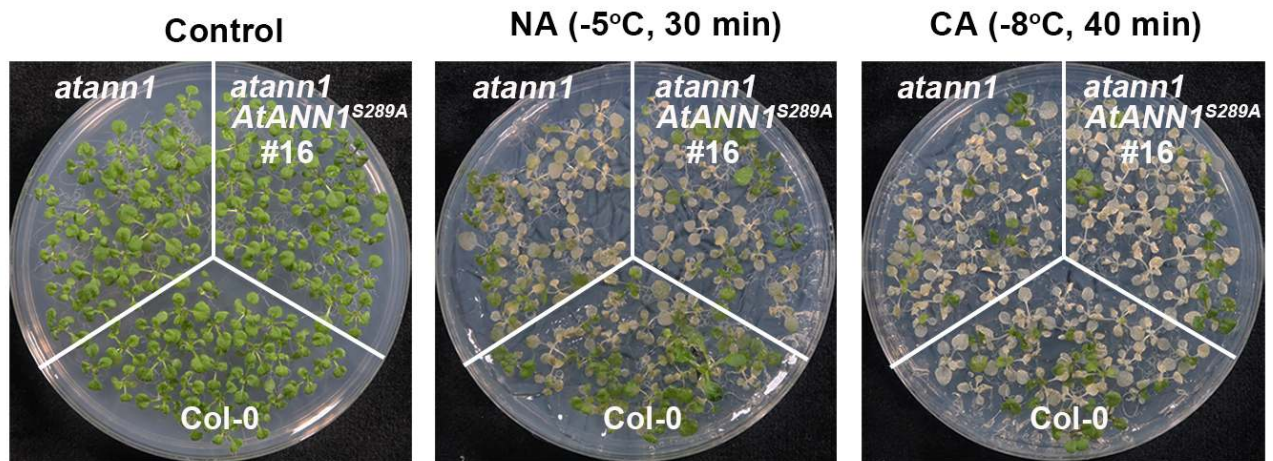
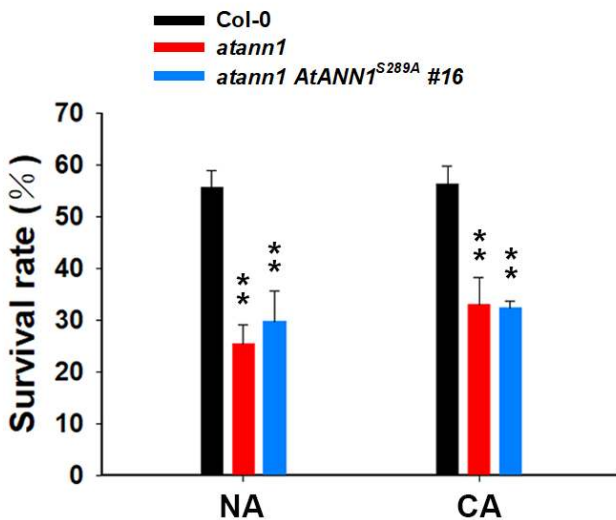
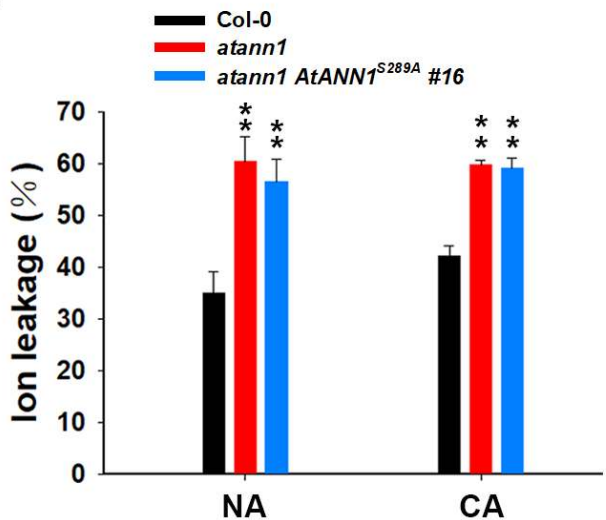


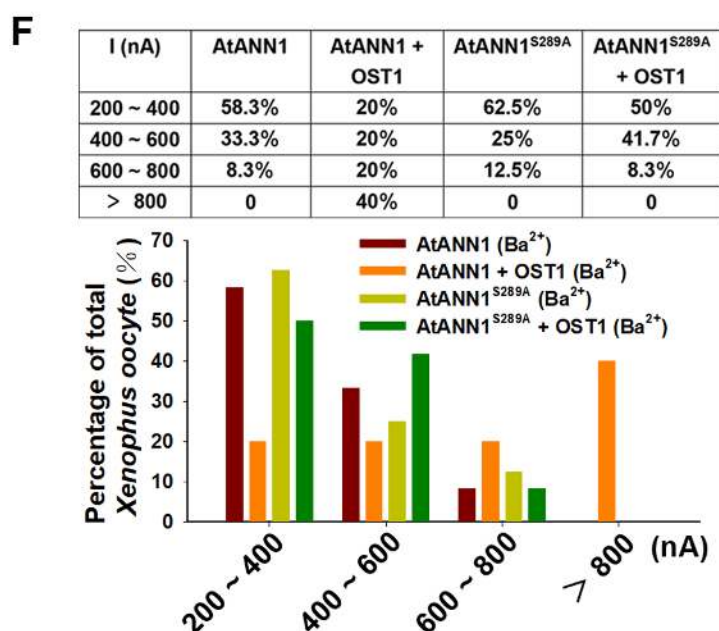
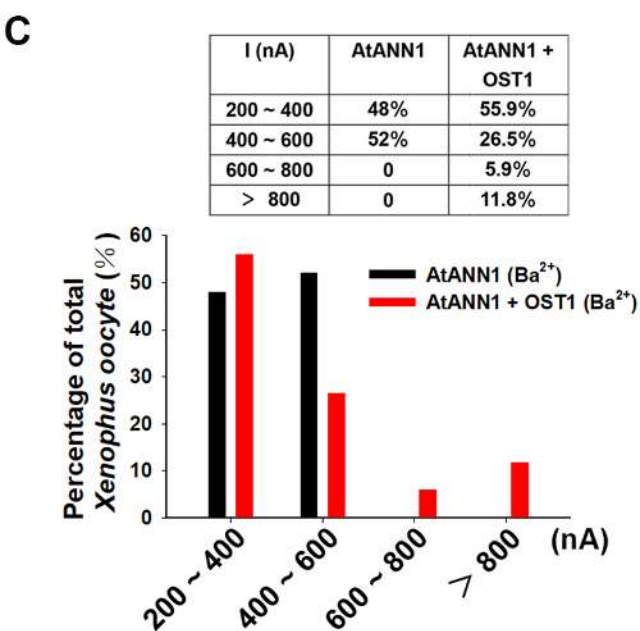
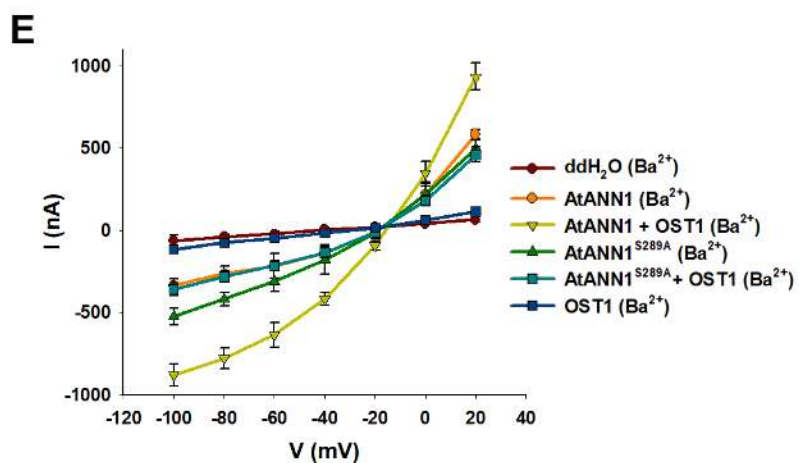
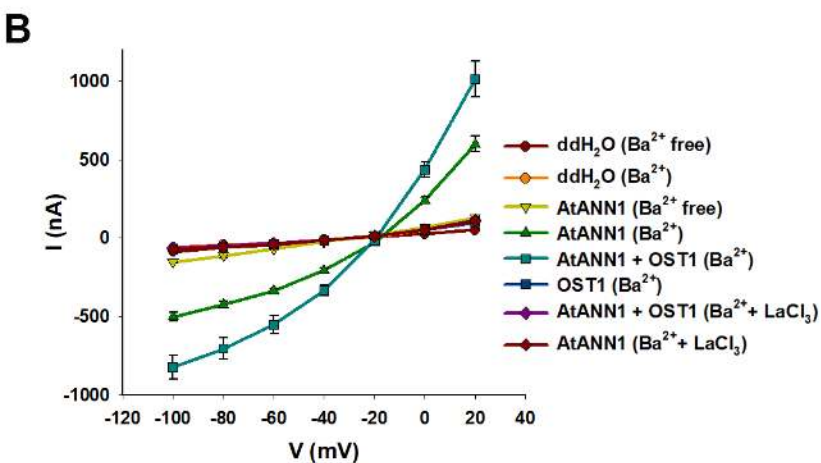
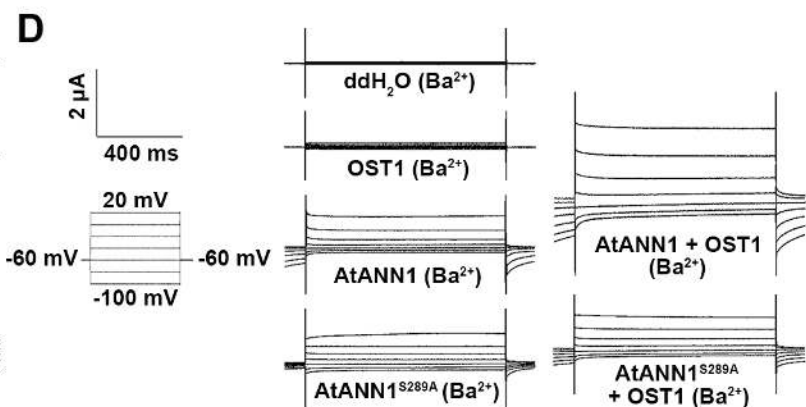
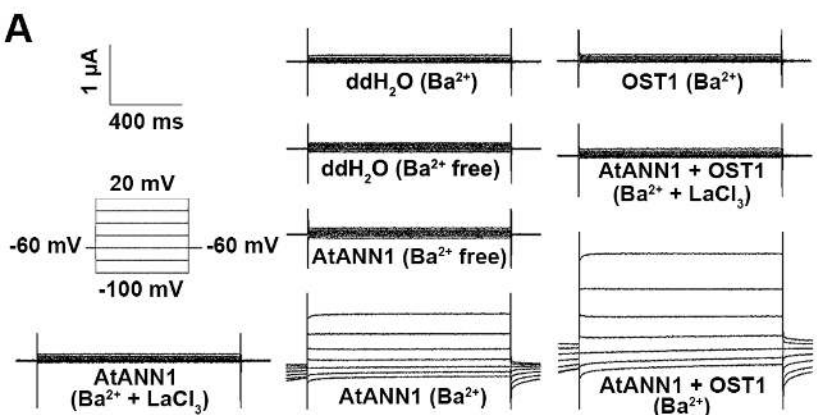


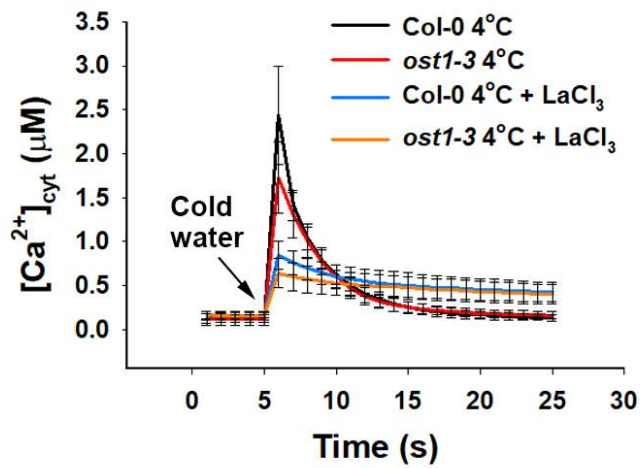
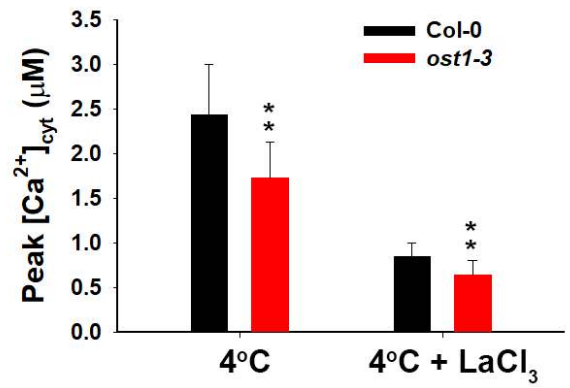
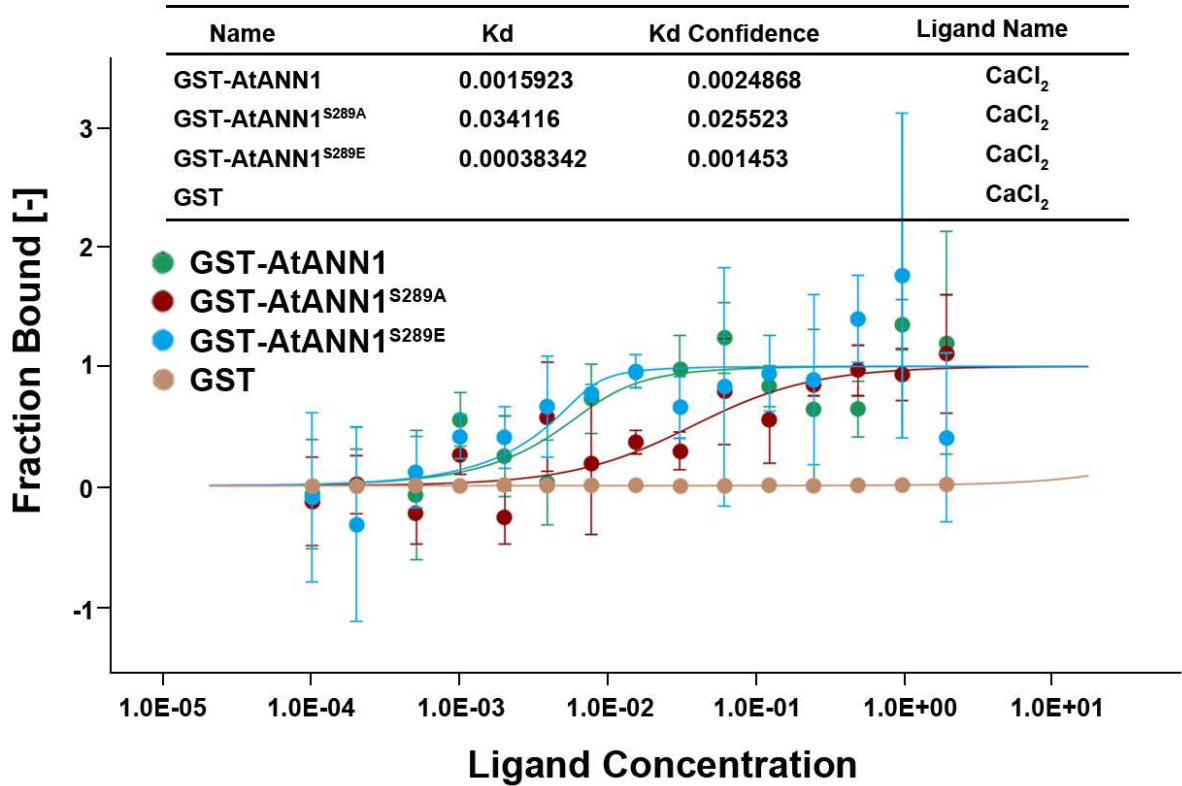
**A****B****C****D****E****F****G****H**





**A****B****C****D****E****F**



**A****B****C****D**